Dtsch. Entomol. Z. 71 (2) 2024, 319–338 | DOI 10.3897/dez.71.134268

PENSOFT

MUSEUM FÜR NATURKUNDE BERLIN

Phylogenetic analysis of the circum-Antarctic Subfamily Migadopinae (Coleoptera, Carabidae) and assessment of the trans-Tasman *Amarotypus* clade

James K. Liebherr[1], Sergio Roig-Juñent[2], Kipling W. Will[3]

1 *Cornell University Insect Collection, Ithaca, NY 14853-2601 USA*

2 *Laboratorio de Entomología, Instituto Argentina de Investigaciones de las Zonas Áridas (IADIZA, CCT–CONICET, Mendoza), 5500 Mendoza, Argentina*

3 *Essig Museum of Entomology, University of California, Berkeley, CA, 94720-3112 USA*

https://zoobank.org/A1638EDA-A566-4837-A558-AA2707FBD0EB

Corresponding author: James K. Liebherr (jkl5@cornell.edu)

Academic editor: Harald Letsch ♦ **Received** 8 August 2024 ♦ **Accepted** 30 October 2024 ♦ **Published** 19 November 2024

Abstract

Phylogenetic analysis of Migadopinae Chaudoir, 1861, based on morphological characters analyzed using maximum parsimony and Bayesian inference, recognizes the tribal adelphotaxa Aquilicini Moret, 2005 and Migadopini. Amarotypini Erwin, 1985 (type genus *Amarotypus* Bates, 1872) is newly synonymized with Migadopini, as its taxonomic recognition renders Migadopini paraphyletic. Phylogenetic relationships within Migadopinae establish the Andean tropicomontane *Aquilex* Moret, 1989—type genus of the monogeneric Aquilicini—as sister group to the circum-Antarctic Migadopini. The earliest-diverging member taxa of Migadopini are distributed across southern South America and the subantarctic Falkland Islands. Subsequent divergence implicates Australia, New Zealand, and the Campbell Plateau. Internodes of the taxon-area cladogram are optimized using RASP (Reconstruct Ancestral State in Phylogenies), with nodal optimizations interpretable by both vicariance or dispersal. Campbell Plateau taxa are ambiguously derived from an ancestral node optimized to either South America, Australia, or the Campbell Plateau itself, a result most consistent with fragmentation of these Gondwanan terranes. Only the origin of the Tasmanian *Migadopiella* Baehr—taxonomically placed within a paraphyletic assemblage comprising the New Zealand genera *Amarotypus*, *Amaroxenus* Larochelle & Larivière, and *Amarophilus* Larochelle & Larivière—is interpreted unambiguously as dispersal based, in this instance via east to west trans-Tasman dispersal. Winged flight by migadopine carabid beetles, previously hypothesized as a vehicle for dispersal between Australia and South America, is dismissed based on restriction of macropterous taxa to two disparate and highly subordinate taxa; one comprising the Australian tropicomontane *Dendromigadops* Baehr and its temperate rainforest-occupying sister genus *Decogmus* Sloane, and the second, *Antarctonomus complanatus* of Valdivian and Magellanic *Nothofagus* forest in Chile and Argentina. Relevant fossil evidence supporting austral relationships of Migadopinae is briefly reviewed, including the mid-Cretaceous occurrence of Migadopinae in Kachin Burmese Amber, and the Miocene-aged fossil carabid beetle, *Antarctotrechus balli* Ashworth and Erwin (Trechini), described from the trans-Antarctic Mountains. The former supports a Cretaceous origin for Migadopinae consistent with Austral vicariance, the latter augurs the discovery of biogeographically homologous Antarctic fossil representatives that could corroborate an Austral vicariance hypothesis for the migadopine radiation.

Key Words

Antarctica, Austral disjunct pattern, biogeography, dispersal, Gondwana, vicariance

Introduction

No topic in historical biogeography has engendered more interest and controversy than the underlying bases for the biotic relationships of the southern continents. Extensive similarities among the floras of New Zealand, Australia, and South America were documented by Hooker (1867); by his estimation, of 303 genera he recognized for New Zealand, 252 also occurred in Australia, and 174 in South America. His explanation for such area relationships was founded on the hypothesis that "*many existing Orders and Genera of plants of the highest development may have flourished during the Eocene and Cretaceous periods, and have hence survived complete revolutions in the temperature and geography of the middle and temperate latitudes of the globe* (Hooker 1859, p. xvii)". Hooker himself immediately offered a counterargument to his hypothesis: "*Mr. Darwin has greatly extended in another direction these views of the antiquity of many European species, and their power of retaining their faces unchanged during most extensive migrations, by his theory of the simultaneous extension of the glacial temperature in both hemispheres, and its consequent effect in cooling the tropical zone* (Hooker 1859, xvii)". Thus, the conventionally-viewed dichotomy of vicariance of ancient biotas surviving revolutions in geography, versus dispersal mediated by climatic changes became established as competing hypotheses explaining the biotic relationships of life on the southern continents. These competing viewpoints are well illustrated by alternate hypotheses proposed to explain diversification of the carabid beetle subfamily Migadopinae Chaudoir, 1861.

Based on Wegener's (1924) hypotheses regarding the past spatial relationships of the continents and oceans, which formed the historical basis for interpreting the climatological observations of Köppen and Wegener (1924), Jeannel (1938) proposed that migadopines originated as early as the Cretaceous on Gondwanan terranes that subsequently became isolated to form present-day southern South America, Australia, New Zealand, and the subantarctic Auckland Islands. Jeannel supported his hypothesis using comparisons of congruent biogeographic patterns in other taxa including, among others, representatives of the carabid subfamilies Broscinae, Bembidiinae tribe Oopterini, and Trechinae tribe Homaloderini (Jeannel 1938: 52). Jeannel's approach accords with Hooker's (1859) view of biogeographic history as revolutionary, with significant changes in both geography and climate underlying historical patterns of diversification.

Darlington (1965), also chose migadopines to exemplify the austral disjunct biogeographic pattern wherein taxa occupy the southern reaches of Australia, New Zealand and South America. He posited that "All faunas are derived. Nowhere in the world is there an existing fauna that cannot be accounted for in terms of derivations from other parts (Darlington 1971: 216)." Moreover, "The history of dispersal of animals seems to be primarily the history of successions of dominant groups, which in turn evolve, spread over the world, compete with and destroy and replace older groups, and then differentiate in different places until overrun and replaced by succeeding groups (Darlington 1959: 488)." In explaining migadopine biogeographic history, he focused on migadopine taxa that occur in subtropical areas, and one—*Decogmus* from subtropical New South Wales, Australia (Baehr 2013)—that retains fully developed metathoracic flight wings in contradistinction to most other migadopine taxa that have reduced, nonfunctional wings. He also noted that Elaphrinae Latreille, 1802, proposed as the closest relatives to Migadopinae by Jeannel (1938), are of Holarctic distribution, necessitating long-distance dispersal from the Northern Hemisphere to account for a southern ancestral distribution for Migadopinae. Darlington also assumed that "the continents and climatic zones have been constant in position during the period under consideration, which is mainly the later Tertiary, Pleistocene, and Recent (Darlington 1959: 489)," thereby requiring migadopines to have dispersed across the Southern Ocean while colonizing Australia, New Zealand and South America.

More recent findings help illuminate the diversification history of Migadopinae. Moret (1989) discovered a remarkable, high-elevation migadopine on Chimborazo, Ecuador—*Aquilex diabolica* Moret—that he proposed as the sister group to all other migadopines. This finding fills in the biogeographic "gap" between migadopines and any Holarctic relatives. Roig-Juñent (2004) conducted a parsimony-based cladistic analysis of migadopines, corroborating Moret's (2005) placement of *Aquilex diabolica*. He also demonstrated the initial radiation of migadopines in South America, with subsequent diversification in Australia and New Zealand. Rogi-Juñent also placed *Amarotypus edwardsii* Bates—type genus of Amarotypini Erwin, 1985—within Migadopini, thereby undercutting cladistic support for tribal status of Amarotypini.

Subsequent advances in taxonomic understanding have been contributed by Johns' (2010) revision of the migadopines of New Zealand, and Baehr's (2009) description of the Tasmanian genus *Migadopiella* Baehr, 2009, followed by his revision of the tribe for Australia (Baehr 2013). Finally, Larochelle and Larivière (2022) revised the New Zealand taxa related to *Amarotypus* Bates, 1872, proposing two new genera—*Amarophilus* Larochelle & Larivière and *Amaroxenus* Larochelle & Larivière—while newly describing 13 species. Their work validates taxa related to those presented informally as "undescribed carabid genus (Johns 1969: 398)", and "New genus, new species A … new species B (Sweney 1980: 107)."

This contribution provides an updated phylogenetic analysis, built on Roig-Juñent (2004), that incorporates additional character information provided by the inclusion of additional outgroup taxa representing the tribe Cicindini Bänninger (Kavanaugh and Erwin 1991), as well as genera described by Baehr (2009, 2013) and Larochelle and Larivière (2022). The resultant cladogram is used to establish a natural classification of Migadopinae wherein monophyletic subtribes and genera are recognized. Multiple generic representatives are included to test the mono-

phyly of the various genera. The phylogenetic hypothesis provides the necessary foundation for historical biogeographic analysis testing whether Migadopinae diversified contemporaneous with fragmentation of Gondwana into its constituent present-day areas of South America, Australia, and New Zealand. Relationships among various subsidiary, and therefore more recently evolved migadopine taxa that occupy Tasmania, New Zealand's South Island, and the Auckland and Antipodes Islands, are interpreted in the context of geological hypotheses in order to ascertain whether vicariance or taxic dispersal better explains these trans-Tasman biogeographical distributions.

Material and methods

Taxonomic material

Specimens were taken on loan for study from the following institutions: Cornell University Insect Collection (**CUIC**), Ithaca, NY, US; Essig Museum of Entomology (**EMEC**), University of California, Berkeley, CA, US; Field Museum of Natural History (**FMNH**), Chicago, IL, US; Lincoln University Entomology Research Collection (**LUNZ**), Lincoln, NZ; Museum of Comparative Zoology (**MCZ**), Harvard University, Cambridge, MA, US; The Natural History Museum (**NHML**), London, UK; New Zealand arthropod Collection, Mt. Albert, NZ (**NZAC**); Tasmanian Museum and Art Gallery (**TMAG**), Hobart, AU; Zoological Museum, University of Copenhagen (**ZMUC**), Copenhagen, DK; Zoologisches Staatssammlung (**ZSM**), München, Bavaria, DE.

Taxonomic protocols

Specimens were examined using a Wild M5 microscope with halogen ring-light illumination at 6–100× magnification. Genitalic dissections were made after specimens were relaxed in hot deionized water containing a few drops of Kodak Photo-Flo® detergent, with the dissections accomplished using modified minutens and watchmakers' forceps. The dissected structures were cleared in 10% cold KOH overnight, then neutralized in dilute acetic acid, and subsequently held in glycerin for viewing and ultimate storage in polyethylene genitalia vials mounted on the specimen pin. Female reproductive tract structures were stained in Kodak Chlorazol Black® suspended in methyl cellosolve after the acetic acid neutralizing step, and then transferred after 15 minutes' staining time to glycerin for viewing. These structures were likewise stored in genitalia vials. Specimen localities were recorded using the area definitions of Crosby et al. (1976).

Body proportions and shapes were quantified using mensural characters determined using an ocular reticle. These include eye size as the ocular ratio MHW / mFW, with MHW being maximal head width across the compound eyes, and mFW is minimum frons width between the compound eyes. Pronotal shape is represented by several ratios—APW / BPW, MPW / BPW, and MPW / PL—where **APW** is apical pronotal width measured at the front angles, **MPW** is maximal pronotal width, **BPW** is basal pronotal width measured between the basal angles, and **PL** is pronotal length measured along the midline. Elytral shape is quantified using HuW / MEW, and MEW / EL; that is **HuW** = width across the humeral angles, **MEW** = maximal elytral width, and **EL** = elytral length measured from the base of the scutellum to the apex of the left elytron. Standardized body size is quantified as the sum of HL + PL + EL, where HL is the midline distance between the anterior margin of the labrum and the ridge demarking the juncture between the vertex and cervix, and PL and EL are as defined above. Migadopines also exhibit variously laterally expanded pro- and mesotarsomeres, that development quantified as the ratio of the maximal lateral breadth of tarsomere 2, divided by the median tarsomere length; w / l. Terminology used for describing male genitalia was based on Lindroth (1957), with Liebherr and Will (1998) followed for interpretation of the female gonocoxae and bursa copulatrix.

Phylogenetic analysis

Cladistic analysis was performed under the maximum parsimony criterion based on a data matrix (Suppl. material 1) comprising 74 characters for 42 taxa (Table 1), this matrix an amended expansion of the 57 character × 29 taxon matrix of Roig-Juñent (2004). The additional taxa principally include those from New Zealand and Australia phylogenetically allied with *Amarotypus edwardsii*. The twenty characters added to the matrix of Roig-Juñent are each indicated below by an asterisk following the character number, while character 43 of Roig-Juñent was deleted as it is autapomorphic. Characters numbered 56 and 57 of Roig-Juñent (2004) were also deleted: 56 because it incorrectly coded *Amarotypus edwardsii* to lack the setose sensillum of the apical gonocoxite, and 57 because a helminthoid sclerite as defined by Liebherr and Will (1998) is not present in migadopine taxa. The resultant matrix was originally edited and entered using Winclada ver. 1.00.08 (Nixon 2002) and subsequently imported into Mesquite ver. 3.81 (Maddison and Maddison 2023b). Using Mesquite, the matrix was submitted to TNT (Goloboff and Morales 2023) with the Zephyr ver. 3.31 (Maddison and Maddison 2023a) package for both parsimony tree and jackknife resampling searches. Tree search was done using Mesquite's default commands for TNT modified to as follows: "Hold" increased to 1000000, "replic" set to 1000, and tbr used "nofillonly". For jackknife analysis Mesquite's default commands for TNT were used and 1000 replications were done. Tree statistics- CI, RI, and length- are given as reported by Mesquite.

The newly amended matrix was also analyzed using Bayesian inference. Bayesian analysis was run under a symmetric model in which the frequen-

Table 1. Outgroup and ingroup taxa analyzed cladistically, with Migadopinae tribal classification consistent with results of this analysis. Generic authorship is provided for genera of Migadopinae.

Cicindinae	
Archaecicindis spp.[1]	
Cicindis horni Bruch	
Elaphrinae	
Blethisa multipunctata L.	
Elaphrus clairvillei Kirby	
Loricerinae	
Loricera foveata LeConte	
Migadopinae	
Aquilicini	
Aquilex Moret	
Aquilex diabolica Moret	
Migadopini	
Migadops Waterhouse	
Migadops jeanneli Nègre	
Migadops latus (Guèrin-Méneville)	
Rhytidognathus Chaudoir	
Rhytidognathus ovalis (Dejean)	
Rhytidognathus platensis (Roig-Juñent & Rouaux)	
Migadopidius Jeannel	
Migadopidius bimaculatus (Reed)	
Lissopterus Waterhouse	
Lissopterus hyadesi Fairmaire	
Lissopterus quadrinotatus Waterhouse	
Pseudomigadops Jeannel	
Pseudomigadops ater Straneo	
Pseudomigadops darwini (Waterhouse)	
Pseudomigadops falklandicus (Waterhouse)	
Pseudomigadops nigrocoeruleus (Waterhouse)	
Pseudomigadops ovalis (Waterhouse)	
Antarctonomus Chaudoir	
Antarctonomus complanatus (Blanchard)	
Monolobus Solier	
Monolobus ovalipennis Straneo	
Monolobus testaceus Solier	
Nebriosoma Laporte de Castelnau	
Nebriosoma fallax Laporte de Castelnau	
Decogmus Sloane	
Decogmus chalybeus Sloane	
Calyptogonia Sloane	
Calyptogonia atra Sloane	
Dendromigadops Baehr	
Dendromigadops gloriosus Baehr	
Amarotypus Bates	
Amarotypus edwardsii Bates	
Amarotypus murchisonorum Larochelle & Larivière	
Amaroxenus Larochelle & Larivière	
Amaroxenus embersoni Liebherr & Will, sp. nov.	
Amaroxenus marrisi Liebherr & Will, sp. nov.	
Migadopiella Baehr	
Migadopiella convexipennis Baehr	
Migadopiella octoguttata Baehr	
Amarophilus Larochelle & Larivière	
Amarophilus otagoensis Larochelle & Larivière	
Amarophilus rotundicollis Larochelle & Larivière	
Stichonotus Sloane	
Stichonotus piceus Sloane	
Stichonotus decoloratus Baehr	
Stichonotus limbatus Sloane	
Stichonotus leai Sloane	
Calathosoma Jeannel	
Calathosoma rubromarginatum (Blanchard)	
Taenarthrus Broun	
Taenarthrus capito (Jeannel)	
Loxomerus Chaudoir	
Loxomerus brevis Blanchard	
Loxomerus huttoni (Broun)	
Loxomerus nebrioides (Guèrin-Méneville)	

[1]*Archaecicindis* spp. coded as composite terminal of *A. johnbeckeri* (Bänninger) in Kavanaugh and Erwin (1991) and *A. hormozensis* Azadbakhsh (2020).

cy of each state is equal and all characters informative using MrBayes ver. 3.2.7, (Ronquist et al. 2012). To ensure that an average standard deviation of split frequencies (ASDSF) below 0.01 was achieved (Ronquist et al. 2009), and that likelihood scores and all parameter values reached a stable plateau, an initial analysis was run using the command "stoprule = yes" with "stopval = 0.009998." Tracer (Rambaut et al. 2018) was used to examine trace files resulting from this run and the effective sample size (ESS) of the parameters used to assess convergence and stationarity. The trees in a burn-in period of 25% of the generations were excluded. While the ASDSF went below 0.01 in only 1.2 million generation for the initial analysis, the ESS values for a few parameters were still below 200, the rule of thumb threshold (Nascimento et al. 2017). The stop value command was removed and a second analysis of 6 million generations for four runs of eight chains was conducted. This analysis reached an ASDSF of 0.0087 and all ESS values viewed in Tracer were > 630. The majority-rule consensus tree of post-burn-in trees was calculated to determine Bayesian posterior probabilities (PP) of clades.

Characters

Character states for the 75 characters are listed below. Character number is based on Roig-Juñent (2004), that sequence modified only by additions or deletions. Characters newly used in this analysis are indicated by an asterisk following the character number. Multistate characters are considered non-additive; i.e., the states are unordered.

Character 1: Seta of mandibular scrobe; absent (0), present (1).

Character 2*: Maxillary stipes setation; 1 (0); 2 at base (1); 3, 2 basally, 1 medially (2); 4, 3 basally, 1 medially (3); 5 along length (4); 9 along length (5).

Character 3: Galea of maxillary palps; 2 articles (0), 1 article (1).

Character 4*: Number of setae on mentum; 2 straddling midline near mentum tooth (0), 4, 2 near midline, 2 basolaterally (1), many bordering margins of mentum (2).

Character 5*: Number of setae on submentum; 2 (0), 4 (1), 6 (2), 8 or more (3).

Character 6: Submentum; separated from mentum (0), fused to mentum, at least in central region (1).

Character 7: Mentum tooth; simple, angulate (0), bilobed or blunt with median concavity (1), absent, no forward expansion medially (2).
Character 8: Paraglossae; long (0), distinct (1), undifferentiated (2).
Character 9: Setae of glossal sclerite; four (0), two (1), one (2).
Character 10: Setae of paraglossae; absent (0), present (1).
Character 11: Labial and maxillary palps; elongate (0) short and wide, subrounded (1).
Character 12: Antennae; short, reaching base of elytron (0), long, reaching the basal third of elytra (1), very long, reaching the middle third of elytra (2).
Character 13: First four antennal segments; pubescent from apex of fourth segment (0), glabrous (1).
Character 14: Supraorbital setae; 2 each side (0), only 1 each side (posterior) (1), only 1 each side (anterior) (2), absent (3).
Character 15*: Posterior supraorbital seta; between eyes, anteriad their hind margin (0), at or posteriad hind margin of eyes (1).
Character 16: Neck; present (0), absent (1).
Character 17: Depression bordering hind margin of eye; absent (0), present (1).
Character 18*: Protibial antennal cleaner; isochaetous, longitudinally sulcate, posterior spur subapical (0), anisochaetous, transverse, posterior spur displaced proximally (1).
Character 19: Fourth male protarsomere apex; truncate (0), bilobed, with both lobes equal (1), bilobed, with anterior lobe more developed than posterior (2).
Character 20: Fourth male mesotarsomere; truncate (0), bilobed with anterior lobe more developed than posterior (1).
Character 21: Fourth male metatarsomere; truncate (0), bilobed, with anterior lobe more developed than posterior (1).
Character 22: Male protarsomeres; normally dilated (0), more distinctly dilated (1).
Character 23: Male protarsomeres; 1–3 with adhesive setae (0), 1–4 or 2–4 with adhesive setae (1).
Character 24: Male mesotarsomeres; 1–4 dilated (0), 1–3 dilated (1), not dilated (2).
Character 25: Male mesotarsomeres; without adhesive setae (0), with adhesive setae (1).
Character 26*: Unguitractor plate of fifth tarsomere; with short projection (0), with elongate projection nearly 1/5 length of ungues (1; Fig. 1).
Character 27: Female protarsomeres; not dilated (0), dilated (1).
Character 28: Female protarsomeres; with only 2 rows ventral setae (0), with expansive field of ventral setae (1).
Character 29: Female mesotarsomeres; 1–4 not dilated (0), dilated (1).
Character 30: Female mesotarsomeres; with only 2 rows ventral setae (0), with expansive fields of ventral setae (1).
Character 31*: Protibial apex; moderately expanded (0); robust overall, very broad apically (1).
Character 32*: Anterior pronotal margin; lined with microsetae across breadth (0), microsetae present medially but absent near front angles (1), microsetae absent medially but present near front angles (2)
Character 33*: Posterior pronotal margin; lined with microsetae across breadth (0), microsetae present medially, absent near basal angles (1).
Character 34: Lateral border of pronotum; broad (0), narrow (1).
Character 35: Anterior and posterior breadths of pronotum; of equal or subequal breadth (0), posterior breadth markedly greater than anterior (1).
Character 36: Anterior marginal bead of pronotum; not marked, at least incomplete medially (0), marked, distinct across breadth (1).
Character 37: Form of pronotum; wider before middle with base constricted (0), sides subparallel (1), sides diverging toward the back, width maximal at basal margin (2).
Character 38: Basal pronotal setae; present (0), absent (1).
Character 39: Lateral pronotal setae; present (0), absent (1).
Character 40: Prosternal process; not extended beyond procoxae except as vertical carina (0), extended posteriad procoxae w/o contacting mesosterum (1), dorsally extended posteriad procoxae, overlapping mesosternum (2).
Character 41: Elytral humeri; rounded (0), angulate to right (1).
Character 42: Basal border of elytra; absent (0), present (1).
Character 43: Elytral striae 1–9; absent, reduced to be untraceable on surface (0), discontinuous (1), fine, continuous (2).
Character 44: Punctation of elytral striae 1–9; absent (0), fine (1), distinct (2).
Character 45: Parascutellar stria; short striole (0), extended to apex of elytra (1).

The nomenclature for elytral striae follows the interpretation of homology for the parascutellar striole and stria 1 given by Will (2020). When impressed, the parascutellar striole is directly adjacent to the scutellum on the elytra and typically continuous with the basal marginal border of the elytra. In many Migadopini, the parascutellar striole has the appearance of a stria that is nearly the length of the elytra and joined to stria 1 in the apical third. In such cases the first two apparent intervals have a homologous correspondence to the branches of the 2nd anal vein of the insect wing.

Character 46*: Parascutellar seta; present (0), absent (1).
Character 47: Bases of elytral striae 1 and 2; fused in a common trunk basally (0), not fused, no common trunk (1)
Character 48: Parascutellar stria and elytral stria 1; fused apically (0), not fused (1).
Character 49: Striae 5 and 6; separated at base (0), joined basally (1).
Character 50*: Stem of fused striae 5 and 6; short (0), long (1).
Character 51: Ninth elytral stria; not crimped on the base (0), bent inwards at the base and attached to the eighth (1).

Character 52*: Elytral marginal setae in interval 9; 6–7 (0); 10–14 (1); 16–22 (2).
Character 53: Elytral coloration; uniform, concolorous on disc (0), with subapical patch of reddish color (1).
Character 54: Elytral marginal coloration; margin concolorous to evenly paler apically (0), margin with irregularly undulated pale areas apically (1).
Character 55*: Metathoracic flight wings; present (0), brachypterous, apex extended more than half elytral length (1), reduced, beetles apterous (2).
Character 56: Male aedeagal median lobe base; open ventrally (0), closed ventrally (1).
Character 57: Male median lobe basal carina; absent (0), present (1).
Character 58: Dorsoventral width of median lobe; thin (0), broad (1).
Character 59*: Ostium position at male median lobe apex; on right (ventral) side of lobe (0), on left (dorsal) side of lobe (1); on medial surface of lobe, dorsal when everted (2).
Character 60*: Ostium opening; broad opening on dorsal aedeagal surface (0), constricted, a small opening on aedeagal surface (1).
Character 61: Ventral region of male median lobe apex; straight, narrow (0), expanded euventrally (1).
Character 62: Male left paramere; glabrous (0), with a few setae (1), with many setae (2).
Character 63: Male left paramere; elongate (0), shape more conchoid (1).
Character 64: Male left paramere apex; sclerotized (0), membranous (1).
Character 65 Male right paramere; with 2 apical setae (0), with a row of ventral setae (1), with 2 rows of ventral setae (2).
Character 66: Sclerites X and Y of male aedeagal internal sac; present (0), absent (1).
Character 67: Ramus associated with female gonocoxite 1; absent (0), present (1).
Character 68: Female gonocoxite IX; 2-segmented (0), unsegmented, basal and apical gonocoxite fused (1).
Character 69: Female basal gonocoxite 1 (or basal portion of fused gonocoxites); apparently glabrous, without elongate setae across ventral surface (0), ventral surface covered with setae (1); with apical border of microtrichia (2), with apical border of palmate microtrichia (3).
Character 70*: Female apical gonocoxite (or apical portion of fused gonocoxites); without medioventral ensiform macrotrichia (0), with 4 mediodorsal ensiform macrotrichia (1).
Character 71*: Ligular sclerite of female bursa copulatrix; present (0), absent (1). This sclerotized structure lies on the ventral surface of the common oviduct, and is not associated with the bursal wall.
Character 72*: Ligular sclerite configuration; elongate (0); longitudinal ridges (1); sclerotized plate (2); cockscomb configuration (3). This character coded only for taxa exhibiting state 1, character 71.
Character 73*: Bursa copulatrix tubular diverticulum; absent (0), present (1). This diverticulum is elongate without an apical expansion, and it joins the bursa copulatrix distad the bursal juncture with the common oviduct. It is not interpreted as a primary spermatheca as it does not expand at the distal end, lacks any taenidial coils often observed in a primary spermatheca, and lacks a gland (Liebherr and Will 1998, fig. 3).
Character 74*: Bursa copulatrix basal diverticulum; absent (0), present (1).

Biogeographic analysis

The phylogenetic hypothesis of migadopine taxa was used to establish a context within which historical biogeographic events could be interpreted by converting the taxon cladogram to a taxon-area cladogram wherein all terminals were represented by areas of endemism. The areas of endemism were defined broadly so that migadopine taxa were geographically restricted relative to the scale of the adopted areas of endemism, and thus all terminals could be coded as single areas. For purposes of this analysis, Tasmania was combined with mainland Australia into a single area of endemism (AU), and both South and North Islands of New Zealand were combined into a single area (NZ). The Auckland and Antipodes Islands represent the Campbell Plateau (CP), considered for this analysis to be an area of endemism distinct from New Zealand. South America is considered as three different areas, one located in the northern high Andes of Ecuador, above 4000 m altitude (ESA), a second, in southern South America including mainly subantarctic moorland and *Nothofagus* forest and Patagonian steppes (SSA), and a third Neotropical region (NEO) comprising tropical lowlands that house one ultimate outgroup taxa, *Cicindis horni* Bruch. The two cicindine genera *Cicindis* and *Archaecicindis* were included in the phylogenetic analysis to enhance character polarizations, but the Cicindini–*Archaecicindis johnbeckeri* Bänninger and *C. horni*–represent the Inabresian zoogeographic pattern (Jeannel 1942; Kavanaugh and Erwin 1991) that spans eastern tropical South America to the Persian Gulf east of Africa. The Inabresian Region was vicariated by the opening of the Atlantic Ocean during the Cretaceous, 119–105 Ma (McLoughlin 2001). This pattern is not analyzed further in the biogeographic analysis as the Holarctic outgroups Loricerinae and Elaphrinae, i.e. *Elaphrus* and *Blethisa*, are considered the successive, closest outgroups to Migadopinae.

Nodal optimizations on the taxon-area cladogram (Fig. 8) were calculated by RASP (Yu et al. 2015, 2019) using 1,000,000 cycles of the Bayesian MCMC BBM algorithm. Nodal optimizations were considered unambiguous (unitary) when the maximal probability of any particular optimization exceeded 0.95. When the maximal probability for any particular optimization was less than 0.95, values for all optimizations exceeding 0.01 are presented for interpretation.

Results

Phylogenetic analysis

Parsimony analysis resulted in 16 shortest trees of 276 step-length; CI of 38, RI of 75. Five nodes within the ingroup Migadopinae collapse in the 283-strep strict consensus tree: 1, four *Pseudomigadops* spp. are collapsed into a polytomy.; 2, *Calyptogonia atra* and *Nebriosoma fallax* and the sister taxa *Decogmus chalybeus* and *Dendromigadops gloriosus* are unresolved adelphotaxa to the clade subtended by *Monolobus* spp.; and 4 and 5, three species each of *Loxomerus* and *Stichonotus* comprise tritomies. The equally parsimonious trees also differ in proposed relationships of three outgroups—*Blethisa multipunctata*, *Elaphrus clairvillei*, and *Loricera foveata*—with the consensus tree collapsing the nodes subtending these taxa. Respective monophyly for the four focal genera—*Amarotypus*, *Amaroxenus*, *Migadopiella*, and *Amarophilus*—is supported.

Bayesian analysis resulted in a majority-rule consensus tree consistent with relationships of the parsimony analysis, though the Bayesian consensus tree is less resolved (Suppl. material 2). As parsimony analysis elucidates characters informing the various relationships, and produces a more resolved consensus cladogram, subsequent analysis and discussion is restricted to the parsimony-based hypothesis (Fig. 5)

The results of the cladistic analysis mirror those of Roig-Juñent (2004) in the placement of *Amarotypus*—plus affiliated taxa from Tasmania and the South Island of New Zealand recognized as Amarotypini by Johns (2010) and Larochelle and Larivière (2022)—as a subset of taxa nested within Migadopini. Were Amarotypini retained as a valid taxon, this result would render Migadopini paraphyletic. Therefore Amarotypini Erwin (1985) is synonymized under Migadopini. Erwin's (1985) proposal for Amarotypini was based on the presence in *Amarotypus* of an elongate unguitractor plate at the apex of the fifth tarsomere (character 21; Fig. 1). Though this synapomorphy is unique and distinctive, its occurrence within the heterobathmy of characters evolving during diversification of Migadopinae restricts its phylogenetic significance to the definition of a subsidiary clade within the tribe Migadopini we name the "*Amarotypus* clade."

Monophyly for the family-group names, Migadopinae, Aquilicini, and Migadopini is supported based on the following sets of characters.

Migadopinae. The subfamily is diagnosed by: 1, antennomeres 1–4 glabrous except for apical setae (character 13); 2, presence of a single supraorbital seta in the posterior setal position each side of head (character 14); 3, head without a posterior constriction, or neck (character 16, reversed to presence of a neck in *Monolobus*); 4, lateral and basal pronotal setae absent (characters 37, 38); 5, male aedeagal internal sac sclerites X and Y (as observed in outgroups and Broscini; e.g. Liebherr et al. 2011, fig. 3b) absent (character 66).

Within Migadopinae, *Aquilex diabolica* Moret is placed as the sister group to taxa constituting Tribe Migadopini,

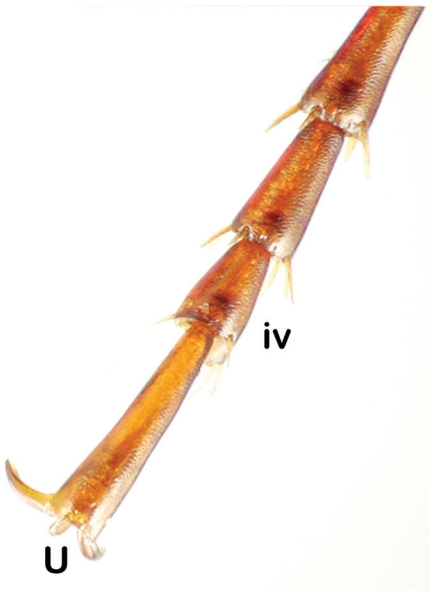

Figure 1. *Amaroxenus marrisi* right metaleg, apical four tarsomeres, showing asymmetrical lobe on anterior of tarsomere 4 (iv), and elongate, digitiform unguitractor plate of apical tarsomere (U).

and thus the status of Aquilicini Moret, 2005 is corroborated. *Aquilex* is excluded from its adelphotaxon Migadopini, as it lacks the elongate parascutellar stria extended beyond elytral mid-length of Migadopini (Moret 2005, fig. 1; character 45). *Aquilex* also shares elongate labial paraglossae (character 8) with the outgroups, whereas members of the Migadopini exhibit shortened paraglossae, most extremely when the paraglossae are not well differentiated from the glossa. The male protarsomeres of *Aquilex* have the basal three tarsomeres bearing squamose setae on the ventral surface as observed in the outgroups, whereas Migadopini have either the four basal tarsomeres with such setae, or tarsomeres 2–4 so clothed (character 23).

Cladistic analysis supports taxonomic recognition of the four genera comprising the *Amarotypus* clade—*Amarotypus*, *Amarophilus*, *Migadopiella* plus *Amaroxenus* (Fig. 5)—via three synapomorphic state changes: 1, presence of four glossal setae (character 9); 2, the uniquely synapomorphous presence of an elongate unguitractor plate of the fifth tarsomere (character 26, Fig. 1); and 3, distinctly punctate elytral striae (character 44), though such punctation is polymorphically present or absent in *Amarophilus murchisonorum* (Suppl. material 1).

Amarotypus stands as sister group to the other three genera, with its monophyly defined by highly derived female gonocoxal morphology, including large macrosetae spanning the juncture between the basal and apical gonocoxite (Fig. 3A), and the presence of four large ensiform mediodorsal setae on the apical gonocoxite (character 70; Fig. 3A). The submentum of *Amarotypus* also exhibits four setae versus the presence of six setae in the other three genera (Larochelle and Larivière 2022) plus *Stichonotus*.

Monophyly of the clade comprising the other three genera—*Amaroxenus*, *Amarophilus*, and *Migadopiella*—is unambiguously supported by: 1, posterior pronotal

margin without microsetae across breadth (character 33); 2, pronotum with subparallel lateral margins (character 35; though *Migadopiella octoguttata* shares a basally broader pronotum with species of *Amarotypus*); 3, female gonocoxite unipartite (character 68; though no female is known for *M. octoguttata*).

Both *Amaroxenus* spp. exhibit a cordate, basally constricted pronotum (character 37, Fig. 2B, C), though such a cordate pronotum also occurs in *Migadopiella convexipennis*. Tarsal characters parsimoniously overrule pronotal shape in this instance, as *Migadopiella* + *Amarophilus* synapomorphously possess a symmetrically bilobed protarsomere 4 (character 19), and a truncate metatarsomere 4 (character 21). Moreover, males of *Migadopiella* spp. synapomorphously exhibit truncate mesotarsomeres 4 (character 20). *Migadopiella* monophyly is also supported by the male aedeagal ostium opening on the left side of the median lobe (character 59; Baehr 2009, fig. 3).

And to conclude, *Amarophilus* monophyly is defined by: 1, the presence of foreshortened antennae that reach the base of the elytra (character 12); and 2, at least partially discontinuous elytral striae (character 43), though this condition is also observed in *Amarotypus edwardsii*. *Amarophilus* spp., in this analysis, are also distinguished by broadly dilated male protarsomeres (character 22, Larochelle and Larivière 2022, fig. 34). That said, the degree of protarsomere dilation in this clade is evolutionarily plastic, with both *Amarotypus murchisonorum* (Larochelle and Larivière 2022, fig. 26) and *Amaroxenus embersoni* (Fig. 2B) of this data set also possessing very broad male protarsomeres.

Taxonomic treatment

Subfamily Migadopinae [as Migadopidae] Chaudoir, 1861: 510 (type genus *Migadops* C. O. Waterhouse, 1842: 136)

Tribe Migadopini Chaudoir, 1861

Monolobina Jeannel, 1938: 13 (type genus *Mololobus* Solier, 1849: 189; synonymy Roig-Juñent, 2004: 12)

Amarotypini Erwin, 1985: 468 (type genus *Amarotypus* Bates, 1872: 50; New Synonymy)

Tribe Aquilicini Moret, 2005: 30 (type genus *Aquilex* Moret, 1989: 246; New Rank)

In order to phylogenetically test the monophyly of the migadopine genera proposed by Baehr (2009) and Larochelle and Larivière (2022), we describe below two species of *Amaroxenus* that complement the species pairs representing *Amarotypus*, *Amarophilus*, and *Migadopiella*.

Amaroxenus Larochelle & Larivière, 2022: 10.

Type species. *Amaroxenus kahurangiensis* Larochelle & Larivière, 2022: 10 (by original designation).

Diagnosis. Within Migadopini exhibiting an elongate parascutellar stria that extends beyond the elytral midlength; mentum medially bidentate, the mentum tooth notched medially; submentum with six setae; pronotum cordate, with basal width subequal to apical width, the lateral margin sinuate anteriad distinct hind angle; pronotal anterior marginal bead usually incomplete medially—in *A. embersoni* sp. nov. polymorphically complete or incomplete medially—always present laterally; metathoracic wings vestigial; pro- and mesothoracic legs with tarsomeres 1–4 laterally expanded in both sexes; female gonocoxite unipartite, the narrower apical portion indistinctly defined relative to the equally sclerotized, broader basal portion, no microtrichia—or a single small seta—situated along the inner margin of the gonocoxite at the point of apical narrowing (Fig. 3B, C).

Diversity. Four species were described by Larochelle and Larivière (2022), to which we add two new species, with the six species determinable using the following key.

Identification key to adults of *Amaroxenus* Larochelle & Larivière

1 Elytral stria 3 with indistinctly developed, fine setiferous punctures. Pronotum subcordate; side moderately rounded; laterobasal fovea not separated from lateral depression by an upraised ridge 2

– Elytral stria 3 with well-developed, coarse setiferous punctures. Pronotum cordate, sides distinctly rounded before sinuate basolateral margins; laterobasal fovea separated from lateral depression by a distinct ridge 4

2(1) Dorsum of body glossy rufopiceous; microsculpture indistinct, a fine transverse mesh on elytra. Pronotal laterobasal foveae moderately broad, shallow, separated from lateral depressions by a pronounced convexity. Elytra distinctly convex; striae shallow, finely punctate, intervals moderately to distinctly convex 3

– Dorsum of body matte brunneous; microsculpture well developed, granulate especially on elytra. Pronotal laterobasal foveae very broad, deep, extended to lateral margins. Elytra moderately convex; striae deep, coarsely punctate, intervals only slightly convex ..... *Amaroxenus glacialis* Larochelle & Larivière

3(2) Pronotum moderately transverse, MPW / PL = 1.29; elytra narrowly ovate, MEW / EL = 0.71; elytra with 14–15 lateral setae in 9th interval bordering lateral marginal depression; standardized body length 6.5—6.6 mm ..... *Amaroxenus arnaudensis* Larochelle & Larivière

– Pronotum broadly transverse, MPW / PL = 1.42; elytra broadly ovate, MEW / EL = 0.76; elytra with 11–13 lateral setae in 9th interval bordering lateral marginal depression; standardized body length 7.8—8.1 mm ..... *Amaroxenus embersoni* Liebherr & Will, sp. nov.

4(1) Antennae brunneous to rufopiceous, apices of antennomeres 5–11 may be darker, but their constricted bases not contrastedly darker than basal four antennomeres; pronotum moderately convex, sides moderately to distinctly sinuate posteriorly, basal angles slightly to distinctly acute, laterobasal foveae very deep; elytra glossy with silvery reflection, moderately to distinctly convex, striae continuous, distinctly punctate 5

– Antennal segments 1–2 rufotestaceous, 3–11 rufopiceous; pronotum distinctly convex, sides not sinuate posteriorly, basal angles rectangular, laterobasal foveae shallow; elytra matte, distinctly convex, striae shallow, finely punctate .... *Amaroxenus huttensis* Larochelle & Larivière

5(4) Elytra moderately convex, disc flat near mid-length mesad stria 4 each side (note parascutellar stria extends between sutural and stria 2), sutural stria finely incised with rudimentary punctures along length on disc; two setae associated with stria 3, both anteriad elytral mid-length; eyes slightly convex, ocular ratio = 1.31 .... *Amaroxenus kahurangiensis* Larochelle & Larivière

– Elytral distinctly and evenly convex, sutural stria deep and smooth on disc; three setae associated with stria 3, the posterior seta just posteriad elytral mid-length; eyes subdepressed, ocular ratio = 1.27 ..... *Amaroxenus marrisi* Liebherr & Will, sp. nov.

Amaroxenus embersoni Liebherr & Will, sp. nov.

https://zoobank.org/45DA3BFE-373C-47A0-B736-B8406053EDAD

Types. ***Holotype*** male (LUNZ) mislabeled: *Arthurs Pass Nat. / Pk, NC 1650 m / Mt. Philistine / 1-i-1988 P. Syrett / R. M. Emberson // under rock / in fine damp / gravel* // HOLOTYPE ♂ / Amaroxenus / embersoni / Liebherr and Will 2023 (black-bordered red label). Based on consultation with Emberson field notes (P. Syrett pers. comm.) the holotype was actually collected at: Arthur's Pass N. P., Mt. Aicken, 1750 m, 1-i-1988 (Fig. 7). ***Paratypes***: same incorrect data label as holotype (LUNZ, 1 ♂); New Zealand: Arthur's Pass N. P., Mt. Aicken, 1750 m, 1-i-1988, R. M. Emberson and P. Syrett, under rock sparse fell field vegetation (LUNZ, 1 ♀) [as noted above, these data are appropriate for all three specimens of *A. embersoni*].

Diagnosis. A broad-bodied species, with transverse pronotum, MPW / PL = 1.42, and broadly ovate elytra, MEW / EL = 0.76 (Fig. 2B); elytra moderately convex but with disc flat; elytral striae punctate in basal ¾ of length, intervals moderately convex on disc; standardized body length 7.8–8.1 mm.

Description. ***Head.*** Frons broad, frontal grooves broad and shallow depressions isolated from clypeus, lined with shallow oblique wrinkles on mesal surface; eyes slightly convex, horizontal diameter intersecting ~20 ommatidia, ocular ratio = 1.28. ***Prothorax*** broadly convex dorsally, middle of disc flat, lateral margins distinctly sinuate anteriad slightly acute hind angles, MPW / BPW = 1.05; basal margin trisinuate, medial margin extended slightly posteriad line intersecting hind angles; base indistinctly, narrowly margined, marginal bead narrowest posteriad laterobasal depression; median base smooth, with shallow ovoid depression at midline; laterobasal depressions broad, defined mesally by irregular declivity, surface dimpled laterad declivity and depression curved upward to broadly meet the narrow lateral margin; median impression very fine, intersecting ~12 fine, transverse impressions that represent little more than irregularities in microsculpture; lateral marginal bead narrowly upraised, lateral marginal depression very narrow and immediately abutting convex disc; anterior margin with distinct, broad lateral bead laterally, but margin nearly smooth medially, margin traceable only in certain orientations of light source; front angles acute, inner margin adhering to lateral surface of head, APW / BPW = 0.74; prosternum smooth medially, lateral reaches slightly undulated; posterior margin of prosternal process extended as adze-like projection, its ventral surface bearing a deep longitudinal declivity; proepisternum / proepimeron juncture lined with ~7 rugose longitudinal depressions. ***Elytra*** narrow basally, HuW / MEW = 0.59, humeri evenly expanded posteriad narrowly rounded humeral angle defined by basal and lateral margins; elongate parascutellar stria joined basally to stria 2, the fused trunk curved laterally parallel to sutural stria; parascutellar stria free apically, terminated at 0.70× elytral length; elytral stria 2 extended nearly to apex, finely punctate even apically, striae 3–6 progressively shorter on apex, stria 7 fused both basally and apically to stria 8, both striae distinctly punctate anteriad posterior juncture, stria 8 irregularly punctate posteriad juncture; stria 9—i.e. lateral marginal depression—punctate nearly to juncture of striae 7 and 8; elytral interval 3 bearing two very fine setae in obscure depressions set at and posteriad elytral mid-length, the impressions situated just mesad stria and associated with slight deviations in the strial orientation; 11–13 lateral elytral setae situated just laterad stria 8. ***Pterothorax*** foreshortened, mesepisternum broadly punctate, with ~20 punctures in posterior 2/3 of length; mesosternum smooth, with fine median crest aligned with adze-like prosternal projection; mesepimeron a narrow longitudinal strap bordering posterior margin of mesepisternum, both sclerites reaching disjunct mesothoracic coxal cavity; metepisternum irregularly quadrate, anterior and posterior margins parallel, medial margin concave along juncture with mesosternum; lateral reaches of metasternum punctate, ~8 punctures over surface. ***Abdomen*** finely punctate basally on first visible ventrite; lateral reaches of ventrites 2–3 longitudinally wrinkled, ventrites 4–6 very finely punctulate over surface; apical ventrite of one male and the female specimen with one seta each side of midline, second male with two setae on right, and one on left side of the ventrite. ***Legs*** with expanded tarsomeres on pro- and mesothoracic legs; males with protarsomere 2 w / l = 1.33, mesotarsomere 2 w / l = 1.04, and females with protarsomere 2 w / l = 1.37,

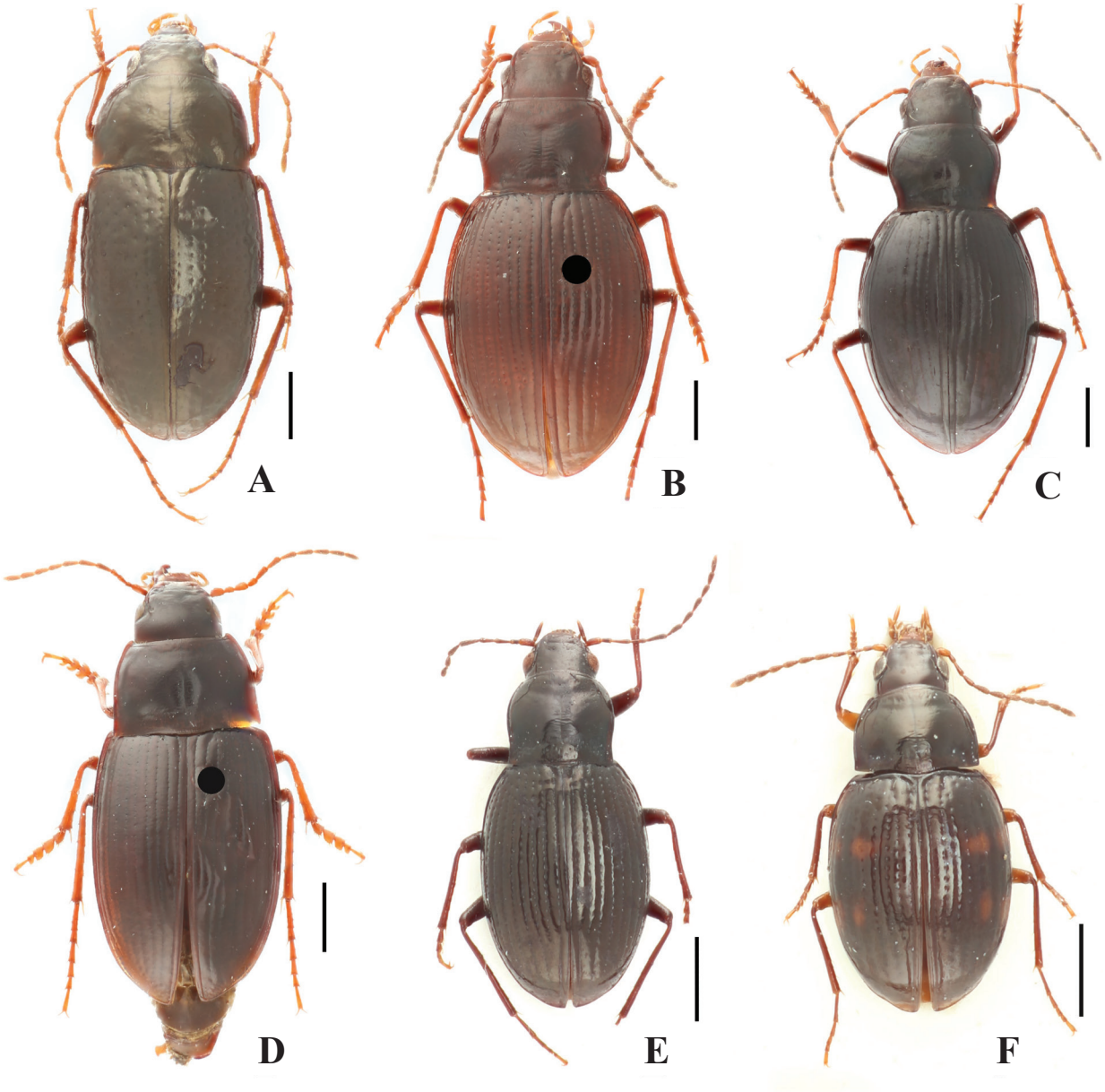

Figure 2. Representative taxa of the *Amarotypus* clade, dorsal view. **A.** *Amarotypus edwardsii*; **B.** *Amaroxenus embersoni*; **C.** *Amaroxenus marrisi*; **D.** *Amarophilus otagoensis*; **E.** *Migadopiella convexipennis*; **F.** *Migadopiella octoguttata*.

mesotarsomere 2 w / l = 0.81; male pro- and mesotarsomeres 1–4 both with ventral surfaces clothed with laterally expanded setae, those on protarsomeres 1–3 broadly expanded laterally, squamose; female protarsomeres 1–4 and mesotarsomeres 2–4 clothed with dense, apical fields of thick, silky, presumably flexible setae.

Male genitalia (Fig. 6A–C). Aedeagal median lobe robust, broad dorsoventrally and bilaterally from base to apically rounded apex (Fig. 6A, B), median lobe basal bulb closed, bearing an apically divergent sagittal crest; median lobe sclerotized basally, ostium opening apically on left side; right paramere broadly conchoid, parallel sided with narrowly rounded ventral apex, ventral margin lined with 3 dense rows of long setae; left paramere conchoid, parallel sided, glabrous, acuminate apicoventrally (Fig. 6B); aedeagal internal sac with heavily sclerotized fields including a dorsal flagellum and a dense ventral spicular field (Fig. 6A); mediotergite VIII broadly rounded distally, sclerotized apex broadened relative to tubular lateral margin (Fig. 6C).

Female reproductive tract. Gonocoxite narrow, elongate, unipartite, articulated basally with heavily sclerotized median boss along anterior margin of laterotergite IX (Fig. 3B); two nematiform setae in apical sensorial pit; ventroapical surface of gonocoxite lined with campaniform sensoria, with several small trichoid sensilla in median half of coxite; bursa copulatrix circular (when compressed on microslide), with common oviduct-bursal juncture on ventral surface, and cristate "helminthoid sclerite" near juncture (Fig. 4B); ventroapical surface of bursa broadly, moderately sclerotized, resulting in a discrete plate just distad the bursal-oviduct juncture.

Etymology. We take great pleasure in naming this species for Professor Rowan M. Emberson (Fig. 7), late

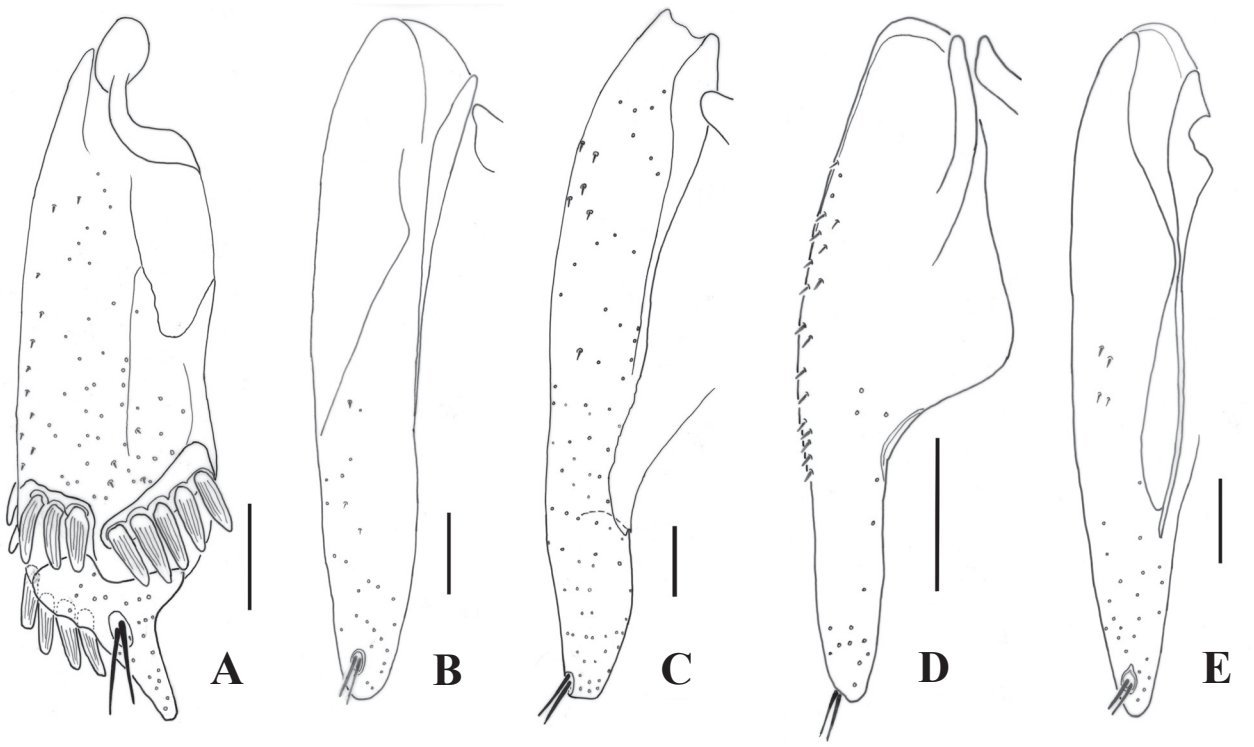

Figure 3. Female left gonocoxite, ventral view. **A.** *Amarotypus edwardsii*; **B.** *Amaroxenus embersoni*; **C.** *Amaroxenus marrisi*; **D.** *Migadopiella octoguttata*; **E.** *Amarophilus otagoensis*.

of Lincoln University. He collected the three type specimens during a hike, accompanied by Pauline Syrett, to the summit of Mt. Aicken in the Southern Alps of New Zealand, December, 1987. The species epithet recognizes Professor Emberson's dedication to the study of New Zealand's insects, including discovery of this high montane New Zealand insect species comprising animals that live in extreme situations far beyond the limits of most entomological exploration.

Distribution. Mt. Aicken is located at 42°55.85'S, 171°35.70′E, and has a summit elevation of 1859 m (https://climbnz.org.nz/nz/si/arthurs-pass/mt-aicken).

Habitat. This is a species of high montane grassland and exposed glacial till. At elevations of 1650–1750 m in the Southern Alps, these habitats are strictly alpine in character. The three specimens were collected under rocks at the edge of receding snowfields (Fig. 7)

Amaroxenus marrisi Liebherr & Will, sp. nov.

https://zoobank.org/38EA8D51-2C05-4BA5-AAD2-705A5FBAFA19

Types. ***Holotype*** male (LUNZ): New Zealand BR / Ridge above Mt. Cedric, 1695 m / GPS 41°53.380S, 172°43.520E / 13 Dec 2008, J. W. M. Marris / Under rock in outcrop // ♂ // HOLOTYPE ♂ / Amaroxenus / marrisi / Liebherr and Will 2023 (black-bordered red label). ***Paratypic allotype*** female (LUNZ): same data as holotype // ♀ // ALLOTYPE ♀ / Amaroxenus / marrisi / J.K. Liebherr 2023 (black-bordered red label). ***Paratypes***: New Zealand, Buller, Nelson Lakes N. P., ridge ENE Mt. Cedric, 1698 m, 41°53.36'S, 172°43.50'E, 13-xii-2008, J. K. Liebherr, under fractured graywacke on moist ground, snowmelt (CUIC, 2 ♂♂, 2 ♀♀; NZAC, 1 ♂, 1 ♀).

Diagnosis. Pronotum slightly transverse, MPW / PL = 1.27, narrower than prothorax of the similar *A. kahurangiensis* with MPW / PL = 1.39; eyes small, indistinctly convex, ocular ratio = 1.27, versus ocular ratio = 1.31 for *A. kahurangiensis*; parascutellar stria and stria 2 punctate, continuous on disc, versus shallower, finely incised with smaller, isolated punctures in *A. kahurangiensis*; three dorsal elytral setae set just mesad stria 3, the anterior two at 0.25× and 0.34× elytral length, the posterior seta posteriad mid-length, near 0.57× elytral length versus only two dorsal elytral setae set before elytral mid-length in *A. kahurangiensis*; standardized body length = 6.9–7.4 mm, tending larger in the extreme than *A. kahurangiensis* at 6.9–7.05 mm. [Note that this size range, based on a male and female (LUNZ) from the same series as the types (Larochelle and Larivière 2022: 13), were measured using the protocol described above. Even though the landmarks used in this study deviate little from those suggested for measuring body length in the works of Larochelle and Larivière (e.g., 2007, fig. 119), our body length measurements for *A. kahurangiensis* are significantly greater than the 5.3–6.6 mm value reported in Larochelle and Larivière 2022).

Description. ***Head.*** Frons broad, flat, with only very shallow frontal impressions traceable each side of midline, middle of frons narrowly flattened, with shallow wrinkles obliquely emanating from flat area approaching the shallow frontal impressions; eyes with horizontal diameter

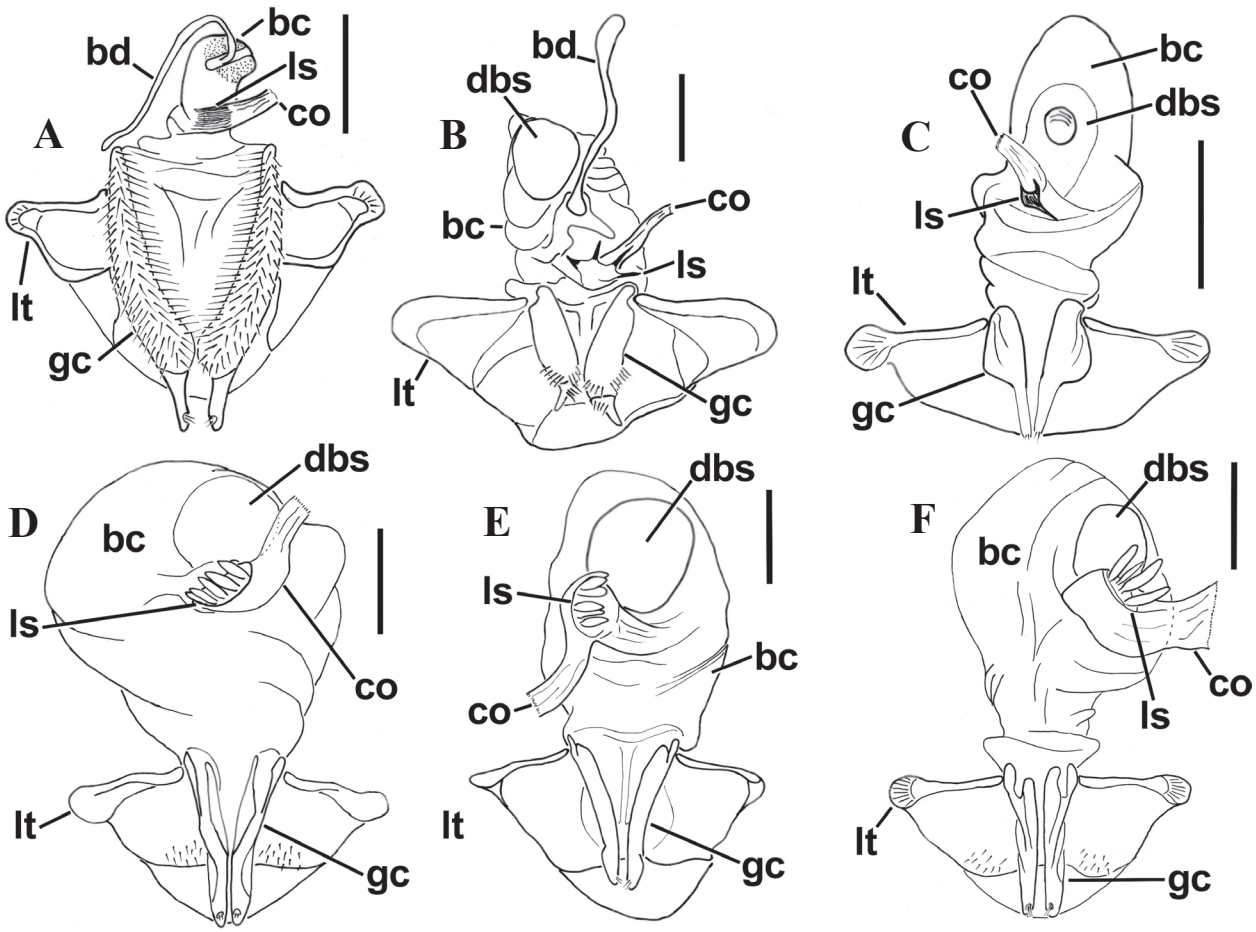

Figure 4. Female reproductive tract, ventral view, scale bar = 0.5 mm to right of each figure. **A.** *Stichonotus piceus*; **B.** *Amarotypus edwardsii*; **C.** *Migadopiella octoguttata*; **D.** *Amaroxenus embersoni*; **E.** *Amaroxenus marrisi*; **F.** *Amarophilus otagoensis*. Abbreviations for anatomical structures include: bc, bursa copulatrix; bd, bursal diverticulum; co, common oviduct; dbs, distal bursal sclerite; gc, gonocoxa; ls, ligular sclerite; lt, laterotergite.

intersecting ~20 ommatidia. ***Prothorax*** broadly convex dorsally, middle of disc flat, lateral margins moderately sinuate anteriad slightly obtuse hind angles, MPW / BPW = 1.11; basal margin trisinuate, medial margin extended slightly posteriad line intersecting hind angles; base with distinct, narrow marginal bead medially, bead less upraised and flatter laterally but continuous to hind angle; median base smooth, convex; laterobasal depressions ovoid, defined mesally by a smooth declivity, surface of depression smooth, only slightly dimpled, depression isolated from lateral margin by broad convexity; median impression very finely inscribed on elevated disc, intersecting ~5 broad transverse impressions between elevated disc and median base; lateral marginal bead very narrow, only slightly upraised, lateral marginal depression exceedingly narrow and immediately abutting convex disc; anterior margin with broad, irregularly flattened lateral bead in medial 4/5 of breadth, distinctly upraised only immediately mesad front angles; front angles acute, inner margin adhering to the lateral surface of the head, APW / BPW = 0.86; prosternum smooth medially, lateral reaches slightly depressed anteriad prosternal-proepisternal suture; posterior margin of prosternal process extended as adze-like projection, its ventral surface bearing a narrow longitudinal declivity that deepens toward apex of projection; proepisternum / proepimeron juncture lined with ~5 rugose longitudinal depressions. ***Elytra*** narrowly ovate, MEW / EL = 0.74, narrow basally, HuW / HEW = 0.58, humeri narrowly expanded posteriad rounded humeral angle defined by basal and lateral margins; elongate parascutellar stria free from stria 2 at basal groove; parascutellar stria free apically, terminated at 0.73× elytral length; elytral stria 2 obsolete near elytral apex, impunctate and discontinuous apicad termination of parascutellar stria, striae 3–7 progressively reduced on apex, discontinuous to obsolete, stria 8 a discontinuous series of distant punctures near humerus, punctures more closely set near mid-length, stria shallow and impunctate in apical half of elytra; stria 9—i.e. lateral marginal depression—closely set with ~10 punctures posteriad humerus, minutely punctate at mid-length and smooth apically; 11–13 lateral elytral setae situated just laterad stria 8. ***Pterothorax*** foreshortened, mesepisternum broadly, shallowly punctate with ~16 punctures across surface; mesosternum smooth, with narrowly cristate median crest aligned with prosternal projection; mesepimeron a narrow parallel-sided strap bordering posterior margin of mesepisternum, both sclerites broadly reaching disjunct mesothoracic coxal

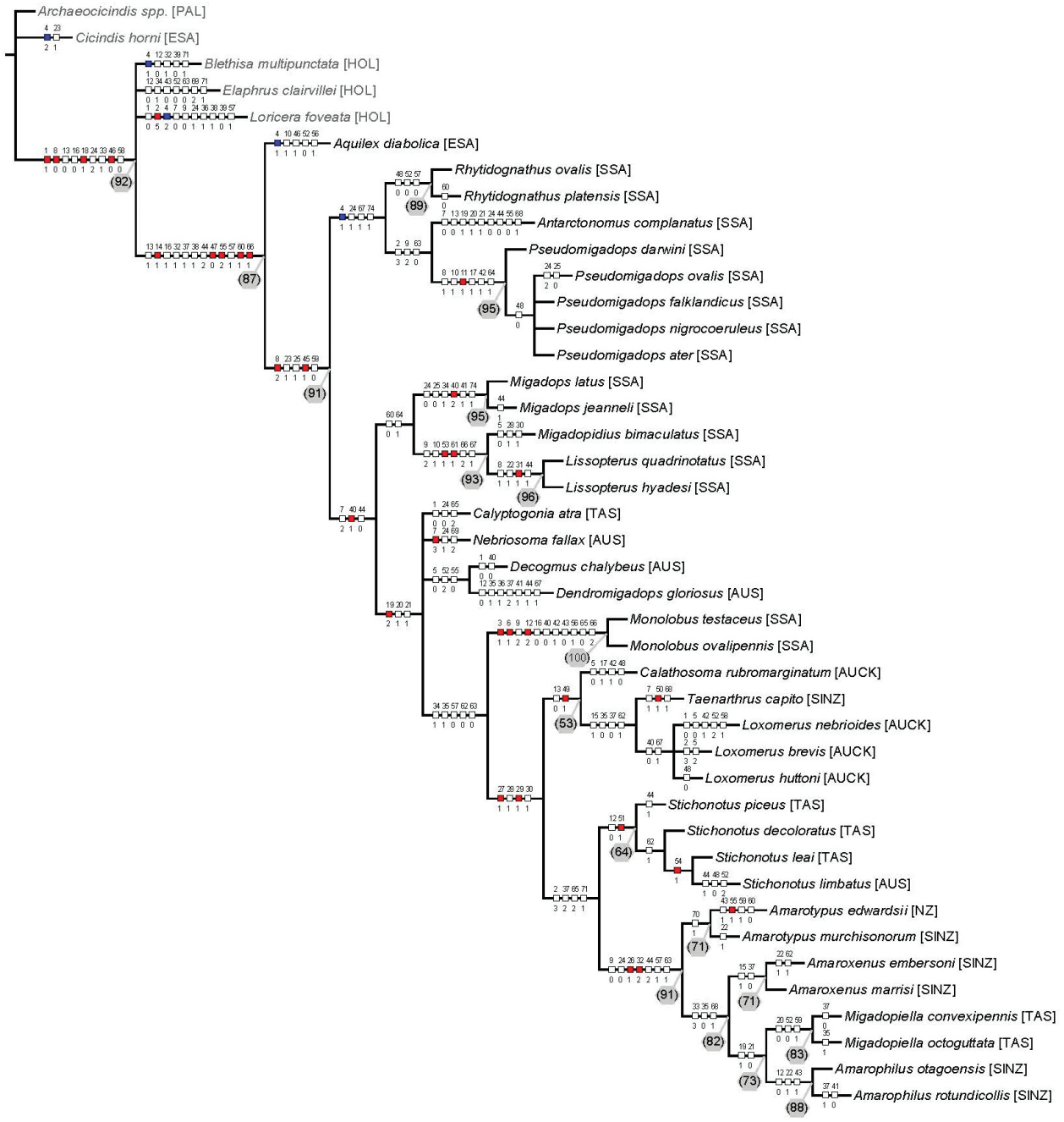

Figure 5. Strict consensus cladogram for Migadopinae plus five outgroup taxa representing Cicindinae, Elaphrinae, and Loricerinae; length 282 steps, CI = 37, RI = 74, with characters indicated under unambiguous optimization option; characters numbered starting with 1; grey spots with Jackknife numbers for nodes with scores ≥ 50; red = not homoplasious; white = homoplasious; blue = deltran character optimization. Areas of endemism occupied by the various taxa include: AUCK, Auckland and Antipodes Islands; AUS, mainland Australia; ESA, equatorial tropicomontane South America; HOL, Holarctic; NEO, Neotropics; NZ, North and South Islands, New Zealand; PAL, Palearctic; SINZ, South Island, New Zealand; SSA, southern South America; TAS, Tasmania.

cavity; metepisternum subquadrate, appearing slightly longer than broad due to concave medial margin along juncture with mesosternum, surface undulated with ~5 minute punctures near medial margin; lateral reaches of mesosternum irregularly undulated along metacoxal juncture. ***Abdomen*** with first visible ventrite smooth, slightly longitudinally wrinkled; lateral reaches of ventrites 2–3 longitudinally wrinkled; ventrites 4–6 smooth except for broad depression halfway between abdominal articulatory setae and lateral margin; apical ventrite of both males and females with one seta each side of midline. ***Legs*** with expanded tarsomeres on pro- and mesothoracic legs; males with protarsomere 2 w / l = 1.2, mesotarsomere 2 w / l = 1.0, and females with protarsomere 2 w / l = 1.37, mesotarsomere 2 w / l = 0.81; male pro- and mesotarsomeres 1–4 both with ventral surfaces clothed with laterally expanded setae, those on protarsomeres 1–3 broadly expanded laterally, squamose, those on tarsomere

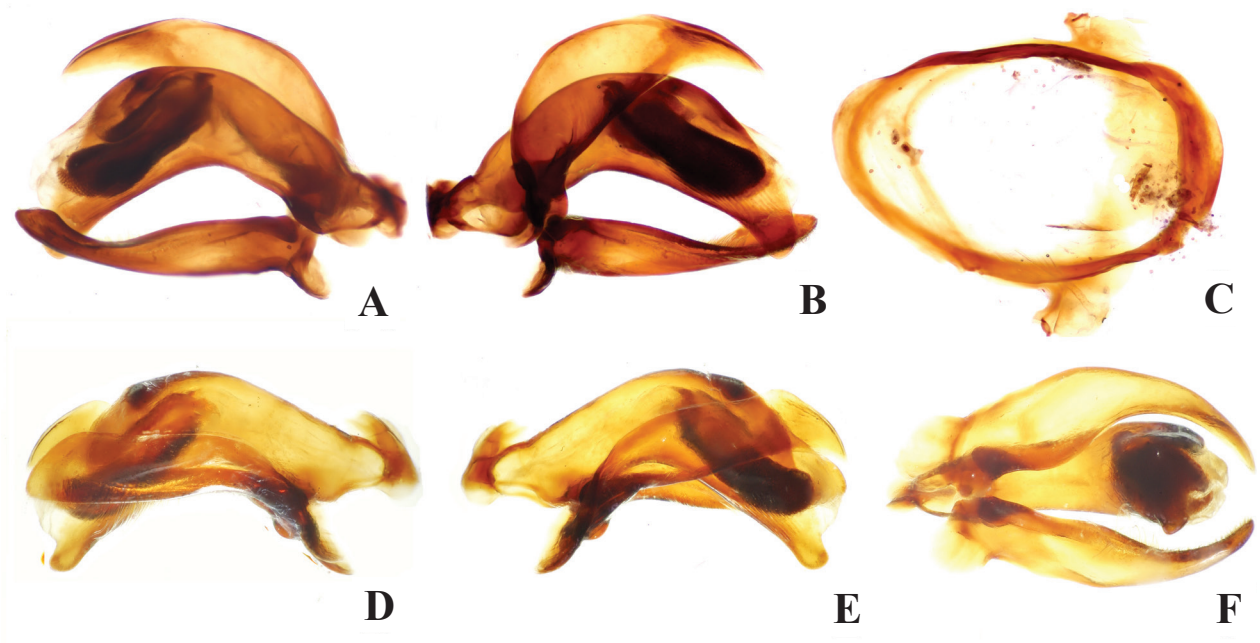

Figure 6. Male aedeagal complex. **A–C.** *Amaroxenus embersoni*. **A.** Median lobe and parameres, dextral view; **B.** Median lobe and parameres, sinistral view; **C.** Metatergite, ventral view. **D–F.** *Amaroxenus marrisi*: **D.** Median lobe and parameres, dextral view; **E.** Median lobe and parameres, sinistral view; **F.** Median lobe and parameres, ventral view.

Figure 7. Type locality of *Amaroxenus embersoni* showing Professor Rowan Emberson collecting the type series (photo courtesy Pol Syrett).

4 tightly packed, silky looking; female protarsomeres 1–4 and mesotarsomeres 2–4 clothed with dense, apical fields of thick, silky, presumably flexible setae.

Male genitalia. Aedeagal median lobe robust, broad dorsoventrally and bilaterally from base to narrow, parallel-sided and apically rounded apex (Fig. 6D–F), median lobe basal bulb closed, bearing an apically divergent sagittal crest (Fig. 6D, E); median lobe sclerotized basally, ostium opening apically on left side; right paramere broadly conchoid, parallel sided with narrowly rounded ventral apex, ventral margin lined with three dense rows of long setae (Fig. 6F); left paramere conchoid, parallel sided, glabrous, acuminate apicoventrally (Fig. 6E); aedeagal internal sac with heavily sclerotized fields including dorsal flagellum and a dense ventral spicular field (Fig. 6D).

Female reproductive tract. Gonocoxite narrow, elongate, apparently unipartite, articulated basally with heavily sclerotized median boss along anterior margin of laterotergite IX (Fig. 3B); two nematiform setae in apical sensorial pit; ventral surface of gonocoxite lined with campaniform sensoria, with a small number of trichoid sensilla along the median half of coxite; bursa copulatrix broadly ovoid (when compressed on microslide), with common oviduct-bursal juncture on ventral surface, and cristate "helminthoid sclerite" near juncture (Fig. 4C); ventroapical surface of bursa broadly, moderately

sclerotized, resulting in discrete plate just distad the bursal-oviduct juncture.

Etymology. This species is named to honor John W. M. Marris for his support of New Zealand entomology, including his efforts to document the high elevation alpine insects of New Zealand; among others the very interesting, lichenophilic *Protodendrophagus antipodes* Thomas (Coleoptera, Silvanidae; see Marris et al. 2019).

Distribution. This species is known only from type locality on the ridge above and ENE of Mt. Cedric, in Buller District. The collecting site is along the valley rim above the headwaters of Open Creek south branch, which flows southwest into the Sabine River.

Habitat. Adult beetles were found within cracks of exposed and crumbling blocks of graywacke in an area of recently melted snow, with the rocky substrate still moist. The rocks had been separated through frost action, with the cracks infiltrated by plant roots, thereby providing moist laminar spaces for insect habitation. The *Amaroxenus* beetles were cohabiting the rock crevices along with adults and larvae of *Protodendrophagus antipodes*.

Biogeographic analysis

Cladistic relationships for Migadopinae versus the closest outgroups included in the phylogenetic analysis (Fig. 5)—represented by *Loricera foveata*, *Blethisa multipunctata*, and *Elaphrus clairvillei*—define a biogeographic hypothesis (Fig. 8) that supports initial diversification of Migadopinae in South America (Fig. 8, node 72). This node ancestral to the Migadopinae is optimized at probability 0.93 to the Holarctic (A), interpreted as a South American origin of the Migadopinae with its sister group in Laurasia.

Within South America, *Aquilex* is placed as the adelphotaxon to all other Migadopinae (Fig. 8, node 71), supporting recognition of the two sister tribes Aquilicini and Migadopini. Node 71 is ambiguously optimized (Table 2) as Holarctic (A, 0.29), equatorial montane South America (B, 0.39), or southern South America (C, 0.22).

Subsequently, diversification of the migadopine genera, *Rhytidognathus*, *Antarctonomus*, *Pseudomigadops*, *Migadops*, *Migadopidius*, and *Lissopterus* took place within South America (Fig. 8, subtending nodes 70, 69). The RASP analysis then posits that occupation of Australia by the grade of taxa including *Calyptogonia*, *Nebriosoma*, *Decogmus*, and *Dendromigadops* (Fig. 5) incorporated an ancestral area (Fig. 8, node 68) that can be variously optimized as South America (C, 0.56), Australia (D, 0.23), or the union of South America and Australia (C + D, 0.21) (Table 2).

Such geographic adjacency is reiterated by optimization of node 67 circumscribing the Antipodean areas, Australia, Campbell Plateau, and New Zealand, with ancestral area states including South America (C, 0.74), Australia (D, 0.12), or the union of the two (C + D, 0.10). The Campbell Plateau was isolated (node 66) prior to isolation of Tasmania and New Zealand (node 65), with optimization probabilities of an ancestral area calculated as either Australia (D, 0.61), New Zealand (0.24), or the union of those (D + E, 0.07) (Table 2).

The taxon-area cladogram posits an origin of the Campbell Plateau fauna as sister group to the Tasmanian *Stichonotus* clade and the amarotypine clade rooted in New Zealand. Node 66 subtending this area relationship is variously optimized to Australia (D, 0.29), New Zealand (E, 0.29), or the Campbell Plateau (F, 0.26) (Table 2), suggesting non-hierarchical area relationships of these terranes.

Subsequent optimization of node 65 supports isolation of Australia from New Zealand, with either Australia (D, 0.61), New Zealand (E, 0.24) or a both areas as ancestral (C + D, 0.7) (Table 2). Ancestral area optimizations for both nodes 66 and 65 strongly suggest an independent history for the Campbell Plateau versus New Zealand west of the Alpine Fault; i.e. North Island and western South Island. The New Zealand clade

Table 2. Ancestral state probabilities for nodes of taxon-area cladogram (Fig. 8) where maximal probability of any particular optimization is < 0.95. Areas include: Holarctic (A); equatorial montane South America (B); southern South America (C), Australia (D), New Zealand (E), and Campbell Plateau (F). Nodal-state probabilities are based on 1,000,000 cycles of the RASP Bayesian Binary MCMC (BBM) algorithm (Yu et al. 2019).

Areas	Node No.									
	72	71	68	67	66	65	64	63	62	60
A	**0.93**	**0.29**	< 0.01	< 0.01	< 0.01	< 0.01	< 0.01	< 0.01	< 0.01	< 0.01
AB	**0.01**	**0.03**	< 0.01	< 0.01	< 0.01	< 0.01	< 0.01	< 0.01	< 0.01	< 0.01
AC	< 0.01	**0.02**	< 0.01	< 0.01	< 0.01	< 0.01	< 0.01	< 0.01	< 0.01	< 0.01
B	**0.02**	**0.39**	< 0.01	< 0.01	< 0.01	< 0.01	< 0.01	< 0.01	< 0.01	< 0.01
BC	< 0.01	**0.03**	< 0.01	< 0.01	< 0.01	< 0.01	< 0.01	< 0.01	< 0.01	< 0.01
C	**0.02**	**0.22**	**0.56**	**0.74**	**0.29**	**0.03**	< 0.01	< 0.01	< 0.01	< 0.01
CD	< 0.01	< 0.01	**0.21**	**0.10**	**0.03**	< 0.01	< 0.01	< 0.01	< 0.01	< 0.01
CF	< 0.01	< 0.01	< 0.01	< 0.01	**0.02**	< 0.01	< 0.01	< 0.01	< 0.01	< 0.01
D	< 0.01	< 0.01	**0.23**	**0.12**	**0.29**	**0.61**	**0.02**	< 0.01	**0.02**	**0.93**
DE	< 0.01	< 0.01	< 0.01	< 0.01	< 0.01	**0.07**	**0.07**	**0.06**	**0.11**	**0.06**
DF	< 0.01	< 0.01	< 0.01	< 0.01	**0.02**	< 0.01	< 0.01	< 0.01	< 0.01	< 0.01
E	< 0.01	< 0.01	< 0.01	< 0.01	**0.06**	**0.24**	**0.91**	**0.94**	**0.86**	**0.01**
EF	< 0.01	< 0.01	< 0.01	< 0.01	< 0.01	< 0.01	< 0.01	< 0.01	< 0.01	< 0.01
F	< 0.01	< 0.01	< 0.01	**0.01**	**0.26**	**0.02**	< 0.01	< 0.01	< 0.01	< 0.01

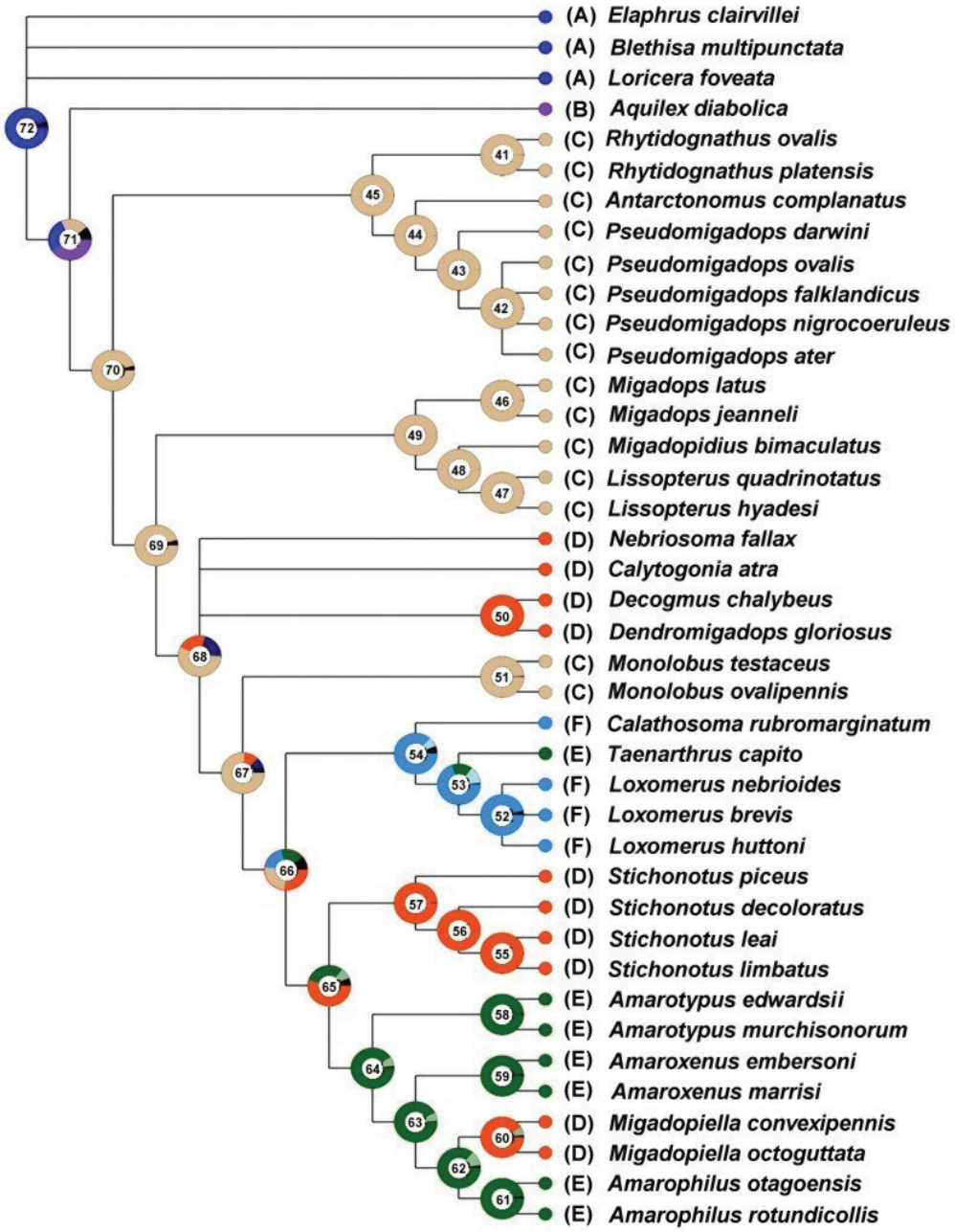

Figure 8. RASP-optimized taxon area cladogram for Migadopinae and closest outgroups in Elaphrinae and Loricerinae. Areas of endemism shown in Figure 5 simplified to allow elucidation of austral disjunct relationships. Areas analyzed include: Holarctic (**A**), equatorial tropicomontane South America (**B**), southern South America (**C**), Australia (**D**), New Zealand (**E**), and Campbell Plateau (**F**). Optimization probabilities for significantly polymorphic nodes—60, 62, 63, 64, 65, 66, 67, 68, 71, 72—in Table 2, other nodes have maximal probabilities of a particular node > 0.95 (optimizations determinable from figure).

rooted with *Amarotypus* sister to the *Stichonotus* lineage of Tasmania and southeast Australia stands as sister to the Campbell Plateau radiation of *Calathosoma*, *Loxomerus*, and *Taenarthrus*.

The most subordinate area relationship connecting New Zealand and Australia is defined by placement *Migadopiella* spp. within the New Zealandian *Amarotypus*, *Amaroxenus*, and *Amarophilus* (node 62, fig. 8). RASP optimizes this node to either New Zealand at probability 0.86, or a combined New Zealand plus Australia at a minority probability of 0.11.

Discussion

Biogeographic History. The closest outgroup Loricerini, represented by *Loricera foveata* LeConte (Fig. 5), is a tribe of Holarctic distribution with extensions southward to the Tibetan Plateau and the mountains of southern Mexico and Middle America (Ball and Erwin 1969). The group was hypothesized to have diversified initially in the Palearctic based on the sister group relationship of the Madeiran *Loricera wollastoni* Javet to the remainder of *Loricera*. The oldest rocks associated with the Tore-Ma-

deira Rise date to the Cretaceous, 80 Ma (Merle et al. 2018), setting a Cretaceous minimum age for loricerine diversification, and by extension the minimum age of the sister group, subfamily Migadopinae (Fig. 8, node 72) isolated by vicariance of Laurasia and Gondwana. Discovery of the Eocene Baltic Amber fossil *Loricera groeni* Cai, Liu and Huang (2017) significantly expanded the paleodistribution of the *Loricera obsoleta* Semenov Tian-Shanskii species group, known to Ball and Erwin (1969) only from the Tibetan Plateau. This recent discovery supports prehistorical sympatry between the *Loricera obsoleta* group currently geographically restricted to the Tibetan Plateau, and the widespread, Holarctic "pilicornis" group that extends southward into Middle America. Subsequent discovery of the fossilized larval stage of the loricerine, *Cretoloricera electra* Liu et al. (2023b), in mid-Cretaceous Kachin amber extends the time of origin of Loricerinae to 99 Ma, thereby setting the time of origin of its adelphotaxon, Migadopinae, to that date.

The sister group relationship between Aquilicini, represented by *Aquilex diabolica*, and Migadopini supports a New World vicariant relationship between the equatorial and southern temperate zones during initial diversification of subfamily Migadopinae (Fig. 8, node 71). The initial divergence of *Aquilex* in equatorial South America versus all other taxa occupying southern South America is represented herein by recognition of the sister tribes Aquilicini and Migadopini.

The biogeographic nexus between South American and Australian taxa (Figs 5, 8) included an initial diversification of the group in Australia—the mid-grade grouping of *Calyptogonia*, *Nebriosoma*, *Decogmus*, and *Dendromigadops* (Fig. 5)—followed by a second radiation of taxa of the Campbell Plateau, New Zealand, and southeastern Australia centered on Tasmania. The initial divergence of the *Calyptogonia* grade in Australia would have occurred with mid-Cretaceous opening of the Australia-east Antarctic rift (Michaux 2009, fig. 2A), allowing secondary dispersal between Australia and east Antarctica to reestablish a cosmopolitan Austral fauna (Fig. 8, node 68).

Monolobus, restricted to the Maule and Valdivian rain forest in Argentina and Chile, is the sister group to the second radiation of Australian and New Zealand taxa (Fig. 8, node 67); i.e., the Campbell Plateau taxa, plus *Stichonotus* of southeastern Australia, and the three New Zealand genera, *Amarotypus*, *Amaroxenus* and *Amarophilus*, plus *Migadopiella* of Tasmania (Fig. 5). The occurrence of a South American Valdivian rainforest taxon that is more closely related to New Zealand and Australian taxa than to other South American taxa was also reported for *Nothobroscus* Roig-Juñent and Ball (Carabidae: Broscinae) (Roig-Juñent 2000, fig. 14; Liebherr et al. 2011, fig. 2). This phylogenetic placement supports the diversification of taxa allied with *Nothobroscus* across a contiguous Gondwana comprising terranes now isolated as southern South America, Australia, the Campbell Plateau and New Zealand.

Isolation between the Campbell Plateau versus New Zealand plus Australia would have been accomplished by mid-Cretaceous along the Campbell Rift (Michaux 2009, fig. 2A), with opening of the Tasman Sea isolating western New Zealand from Australia by late Cretaceous. Although *Taenarthrus*, nested within the Campbell Plateau *Calathosoma* and *Loxomerus* (Fig. 8), comprises species currently occupying the southern portions of the South Island with highest diversity in Fjordland, this region is hypothesized to share a common history with the currently isolated Auckland Islands plus other islands of the Campbell Plateau (Michaux and Leschen 2005).

The area relationship between *Migadopiella* and the New Zealand genera *Amarotypus*, *Amaroxenus* and *Amarophilus* is best explained, within the context of all other biogeographic events, as east to west trans-Tasman dispersal from New Zealand's South Island to Tasmania (node 62; Table 2, Fig. 8). This interpretation is consistent with dispersal being the preferred explanation for the biogeographic origin of a subordinate taxon nested within a larger paraphyletic assemblage of taxa occupying a second area (Enghoff 1993). Such a dispersal event is hypothesized to have occurred in a clade predominantly comprising apterous taxa; the only exception being *Amarotypus edwardsii* which is characterized by brachyptery, with its reduced flight wings extended to 65–75% of elytral length (Larochelle and Larivière 2022: 5). East to west trans-Tasman dispersal hypothesized for *Migadopiella* conforms to findings of Sanmartín and Ronquist (2004, table 4, fig. 9), who reported no significant directionality to trans-Tasman dispersal among insect taxa.

Flightlessness, dispersal and colonization

Darlington (1965) proposed that flight-capable migadopine taxa such as the South American *Antarctonomus* plus the Queensland, Australian *Dendromigadops* represent the ancestral stock of the group, with such winged taxa dispersing between South America and Australia to establish a southern disjunct distribution. Although all three immediate outgroup representatives–*Blethisa multipunctata*, *Elaphrus clairvillei*, and *Loricera foveata* (Fig. 5)–are characterized by macroptery, only the phylogenetically subordinate ingroup taxa *Antarctonomus complanatus*, *Decogmus chalybeus*, and *Dendromigadops gloriosus* exhibit fully developed flight wings. Analogously, *Amarotypus edwardsii* exhibits brachypterous flight-wings—i.e. reduced in length by approximately half—while being placed within a clade otherwise characterized by totally reduced flight wings; aptery. These several instances may be explained by the demonstrably frequent evolution of flightlessness across Carabidae among taxa occupying montane and islandic habitats (Darlington 1943; Kavanaugh 1985), with that repeated evolution violating the principal of parsimony (Trueman et al. 2004). Conversely, re-evolution of fully developed flight wings from apterous ancestors has been argued for Phasmatodea (Whiting et al. 2003; Forni et al. 2022). Regardless, the earliest diverging lineages within Migadopinae are not characterized by macroptery, and so

Darlington's hypothesis of ancestral dispersal by migadopines across open southern oceans is not corroborated.

Darlington's (1965) proposal that ancestral colonizing migadopine taxa were flight capable conforms to an interpretation that dispersal to novel terranes occurs via winged beetles. Yet the trans-Tasman colonization of Tasmania by *Migadopiella* occurred from among a set of wingless taxa. Also, among the Campbell Plateau migadopine taxa, four species—*Loxomerus nebrioides*, *L. katote* Johns, *L. huttoni*, and *Calathosoma rubromarginatum* (Johns 2010)—occupy the Auckland Islands, with that archipelago comprising Miocene shield volcanoes overlying Cretaceous granite (Denison and Coombs 1977), yet the Pleistocene-aged Antipodes Islands (Scott et al. 2013) house the similarly flightless *Loxomerus brevis.* The occurrence of *L. brevis* on the Antipodes is thus best explained by overwater dispersal, with such an instance again occurring within a brachypterous clade.

Fossil corroboration

Based on phylogenetic analysis of extant taxa, we predict future discovery of fossil taxa representing tribe Migadopini from Antarctica. We already have the first example of an Antarctic carabid beetle corroborating a trans-Antarctic biogeographic relationship through the discovery of the fossil, *Antarctotrechus balli* Ashworth and Erwin (2016). In this instance, *Antarctotrechus* is a member of a clade within the tribe Trechini comprising *Trechisibus* Motschulsky of South America, the Falkland Islands and South Georgia, and *Tasmanorites* Jeannel of Tasmania, Australia. The fossil *Antarctotrechus* is dated 20–14 Ma, i.e., Early to Mid-Miocene, well after the Oligocene opening of the Southern Ocean, suggesting that it was part of a fauna already evolving in isolation from related taxa on opposite sides of the southern world. It was deposited in materials consistent with mixed forest and tundra vegetation, including *Nothofagus* (southern beech) and *Ranunculus* (buttercup), indicating a riparian habitat. The present phylogenetic hypothesis incorporating austral Migadopini (Fig. 5) lays out characters that may be evaluated should a fossil Antarctic migadopine become available.

Recently, a much older Cretaceous amber fossil from Myanmar—*Cretomigadops bidentatus* (Liu et al. 2023a)—has been described as a member of Migadopinae based on a first instar larva encased within Burmese Kachin amber dated to 99 Ma. The fossil exhibits synapomorphies characterizing Carabidae, though placement as Migadopinae is based solely on the presence of two retinacular teeth on the mandible; a larger tooth in a plesiomorphic position near mid-length on the mandible, and a second smaller tooth more basad along the medial mandibular margin. Such a second mandibular tooth is reported for third instar larvae of *Loxomerus brevis* and *L. nebrioides* (Johns 1974), as well as larvae of *Omophron* Latreille, Tribe Omophronini (Thompson 1979). The Cretaceous *Cretomigadops* larva differs from *Loxomerus* larvae in: 1, the second, basal mandibular tooth being much larger relative to the distal tooth; 2, the structure of the antennal sensorium; 2, the very long legs; 3, the slender and very elongate urogomphi; and 4, paired ungual claws of equal length. The occurrence of *Cretamigadops* in Kachin amber necessitates additional assumptions concerning the historical biogeography based on extant taxa. Confirmation of a trans-Tethyan migadopine distribution can be corroborated through discovery of fossilized adult Migadopinae in Kachin Amber. Of course, more extensive taxonomic representation of known migadopine larval stages among extant taxa would also allow confirmation that the basal, larval retinacular tooth serves as a synapomorphy for Migadopinae. Given that the phylogenetic nexus between the Laurasian outgroups and Gondwanan Migadopinae occurred across what is now the Neotropics (Crowson 1980; McLoughlin 2001), the phylogenetic position of Burmese Migadopinae is predicted to be sister group to Aquilicini + Migadopini. The above-presented hypothesis for Gondwanan vicariance and trans-Tasman dispersal would remain unaffected, with the Aquilicini + Migadopini hypothesized to have evolved on a fragmenting Gondwana.

Acknowledgements

We thank the following curators for access to research specimens essential to this project (collection codens trailing): Margaret Thayer and Alfred Newton, (FMNH); John W. M. Marris (LUNZ); Crystal Maier (MCZ); Beulah Garner (NHML); Rich Leschen and Grace Hall (NZAC); Simon Grove and Kirrily Moore (TMAG); Alexey Solodovnikov (ZMUC); Michael Balke (ZSM). Pierre Moret collegially shared his knowledge of migadopine characters allowing us to enlarge the phylogenetic matrix, thereby enhancing support for our analysis. We thank Nick Porch and an anonymous reviewer for constructive criticism that led to a substantially improved manuscript.

References

Ashworth AC, Erwin TL (2016) *Antarctotrechus balli* sp. nov. (Carabidae, Trechini): the first ground beetle from Antarctica. ZooKeys 635: 109–122. https://doi.org/10.3897/zookeys.635.10535

Azadbakhsh S (2020) A new species of *Archaeociocindis* Kavanaugh & Erwin, 1991 (Coleoptera: Carabidae: Cicindini) from the south of Iran. Zeitschrift der Arbeitsgemeinschaft Österreichischer Entomologen 72: 37–42.

Baehr M (2009) A new genus and two new species of the subfamily Migadopinae from Tasmania (Coleoptera: Carabidae). Folia Heyrovskyana (series A) 17: 95–103.

Baehr M (2013) [2012] A revision of the carabid tribe Migadopini in Australia (Insecta: Coleoptera: Carabidae: Migadopini). Memoirs of the Queensland Museum-Nature 65(2): 279–304.

Ball GE, Erwin TL (1969) A taxonomic synopsis of the tribe Loricerini (Coleoptera: Carabidae). Canadian Journal of Zoology 47: 877–907. https://doi.org/10.1139/z69-146

Cai C, Liu Y, Huang D (2017) A new species of *Loricera* Latreille from Eocene Baltic amber (Coleoptera: Carabidae: Loricerinae). Alcheringa: An Australasian Journal of Palaeontology 41(3): 315–320. https://doi.org/10.1080/03115518.2017.1283050

Crosby TK, Dugdale JS, Watt JC (1976) Recording specimen localities in New Zealand: an arbitrary system of areas and codes defined. New Zealand Journal of Zoology 3: 69. https://doi.org/10.1080/03014223.1976.9517903

Crowson RA (1980) On amphipolar distribution patterns in some cool climate groups of Coleoptera. Entomologia Generalis 6(2/4): 281–292. https://doi.org/10.1127/entom.gen/6/1980/281

Darlington Jr PJ (1943) Carabidae of mountains and islands: data on the evolution of isolated faunas, and on atrophy of wings. Ecological Monographs 13: 37–61. https://doi.org/10.2307/1943589

Darlington Jr PJ (1959) Area, climate, and evolution. Evolution 13: 488–510. https://doi.org/10.2307/2406131

Darlington Jr PJ (1965) Biogeography of the Southern End of the World, Distribution and history of far southern life and land, with an assessment of continental drift. Harvard University Press, Cambridge, M, x + 236 pp. https://doi.org/10.4159/harvard.9780674492073

Darlington Jr PJ (1971) The carabid beetles of New Guinea. Part IV. General considerations: analysis and history of fauna: taxonomic supplement. Bulletin of the Museum of Comparative Zoology 142(2): 129–337.

Denison RE, Coombs DS (1977) Radiometric ages for some rocks from Snares and Auckland Islands, Campbell Plateau. Earth and Planetary Science Letters 34: 23–29. https://doi.org/10.1016/0012-821X(77)90101-7

Enghoff H (1993) Phylogenetic biogeography of a Holarctic group: the julidan millipedes. Cladistic subordinateness as an indicator of dispersal. Journal of Biogeography 20: 525–536. https://doi.org/10.2307/2845724

Erwin TL (1985) The taxon pulse: a general pattern of lineage radiation and extinction among carabid beetles. In: Ball GE (Ed.) Taxonomy, Phylogeny and Zoogeography of Beetles and Ants, Dr. W. Junk Publishers, Dordrecht, 437–472.

Forni G, Martelossi J, Valero P, Henneman FH, Conle O, Luchetti A, Mantovani B (2022) Macroevolutionary analyses provide new evidence of phasmid wings evolution as a reversible process. Systematic Biology 71: 1471–1486. https://doi.org/10.1093/sysbio/syac038

Goloboff PA, Morales ME (2023) TNT version 1.6, with a graphical interface for MacOS and Linux, including new routines in parallel. Cladistics 39: 144–153. https://doi.org/10.1111/cla.12524

Hooker JD (1859) On the flora of Australia, its origin, affinities, and distribution; being an Introductory essay to the flora of Tasmania (reprinted from the Botany of the Antarctic Expedition, Part III, Flora of Tasmania, Vol. I.). Lovell Reeve, London, cxxviii pp. https://doi.org/10.5962/bhl.title.60980

Hooker JD (1867) Handbook of the New Zealand flora: a systematic description of the native plants of New Zealand and the Chatham, Kermadec's, Lord Auckland's, Campbell's and Macquarrie's Islands. https://doi.org/10.5962/bhl.title.132966

Jeannel R (1938) Les Migadopides (Coleoptera Adephaga), une lignée subantarctique. Revue Française d'Entomologie 5: 1–55.

Jeannel R (1942) La Genèse des Faunes Terrestres, Éléments de Biogéographie. Bibliothèque de l'Institut Maritime et Colonial, Presses Universitaire de France, 513 pp. [+ 8 pls]

Johns PM (1969) The mountain invertebrate fauna. In: Knox GA (Ed.) The Natural History of Canterbury, AH Reed and AW Reed, Wellington, 392–399.

Johns PM (1974) Arthropoda of the subantarctic islands of New Zealand (1) (Coleoptera: Carabidae), southern New Zealand, Patagonian, and Falkland Islands insular Carabidae. Journal of the Royal Society of New Zealand 4: 283–302. https://doi.org/10.1080/03036758.1974.10419396

Johns PM (2010) Migadopini (Coleoptera: Carabidae: Migadopinae) of New Zealand. Records of the Canterbury Museum 24: 39–63.

Kavanaugh DH (1985) On wing atrophy in carabid beetles (Coleoptera: Carabidae), with special reference to Nearctic *Nebria*. In: Ball GE (Ed.) Taxonomy, Phylogeny and Zoogeography of Beetles and Ants, Dr. W. Junk Publishers, Dordrecht, 406–431.

Kavanaugh, DH, Erwin TL (1991) The tribe Cicindini Bänninger (Coleoptera: Carabidae): comparative morphology, classification, natural history, and evolution. Proceedings of the Entomological Society of Washington 93: 356–389.

Köppen W, Wegener A (1924) Die Klimate der geologischen Vorzeit. Gebrüder Borntrager, Berlin, 275 pp. https://doi.org/10.1515/9783111491530

Larochelle A, Larivière M-C (2022) Synopsis of the tribe Amarotypini in New Zealand (Coleoptera: Carabidae). Insecta Mundi 0942: 1–30. https://doi.org/10.5281/zenodo.7300590

Liebherr JK, Will KW (1998) Inferring phylogenetic relationships within Carabidae (Insecta, Coleoptera) from characters of the female reproductive tract. In: Ball GE, Casale A, Vigna Taglianti A (eds.); Phylogeny and classification of Caraboidea (Coleoptera: Adephaga). Atti Museo Regionale de Scienze Naturali 5: 107–170.

Liebherr JK, Marris JWM, Emberson RM, Syrett P, Roig-Juñent S (2011) *Orthoglymma wangapeka*, gen. n., sp. nov. (Coleoptera: Carabidae): a newly discovered relict from the Buller Terrane, northwestern South Island, New Zealand, corroborates a general pattern of Gondwanan endemism. Systematic Entomology 36: 395–414. [3 suppl. appendices]. https://doi.org/10.1111/j.1365-3113.2011.00569.x

Lindroth C (1957) The principal terms used for male and female genitalia in Coleoptera. Opuscula Entomologica 22(2/3): 241–256.

Liu H, Beutel RG, Makarov KV, Jarzembowski EA, Xiao C, Luo C (2023a) The first larval record of Migadopinae (Coleoptera: Adephaga: Carabidae) from mid-Cretaceous Kachin amber, northern Myanmar. Cretaceous Research 142: 105413. [12 pp.] https://doi.org/10.1016/j.cretres.2022.105413

Liu H, Makarov KV, Jarzembowshi A, Xiao C, Luo C (2023b) *Cretoloricera electra* gen. et sp. nov., the oldest record of Loricerini (Coleoptera: Adephaga: Carabidae: Loricerinae) from mid-Cretaceous Kachin Amber. Cretaceous Research 148: 105540. [8 pp.] https://doi.org/10.1016/j.cretres.2023.105540

Maddison DR, Maddison WP (2023a) Zephyr: a Mesquite package for interacting with external phylogeny inference programs. Version 3.31. http://zephyr.mesquiteproject.org

Maddison WP, Maddison DR (2023b) Mesquite: a modular system for evolutionary analysis. Version 3.81. http://www.mesquiteproject.org

Marris J, Hawke D, Glenny D (2019) Eating at high elevation: an herbivorous beetle from alpine rock outcrops relies on ammonia-absorbing lichens. Ecology 100(5): e02598. https://doi.org/10.1002/ecy.2598

McLoughlin S (2001) The breakup history of Gondwana and its impact on pre-Cenozoic floristic provincialism. Australian Journal of Botany 49: 271–300. https://doi.org/10.1071/BT00023

Merle R, Jourdan F, Goirardeau J (2018) Geochronology of the Tore-Madeira Rise seamounts and surrounding areas: a review, Australian Journal of Earth Sciences 65(5): 591–605. https://doi.org/10.1080/08120099.2018.1471005

Michaux B (2009) Reciprocality between biology and geology: Reconstructing polar Gondwana. Gondwana Research 16: 655–668. https://doi.org/10.1016/j.gr.2009.06.002

Michaux B, Leschen R (2005) East meets west: biogeology of the Campbell Plateau. Biological Journal of the Linnean Society 86: 95–115. https://doi.org/10.1111/j.1095-8312.2005.00511.x

Moret P (1989) Un Migadopidae sans stria surnuméraire des Andes de l'Équateur: *Aquilex diabolica* gen. nov., sp. nov. (Coleoptera: Caraboidea). Nouvelle Revue d'Entomologie (N.S.) 6(3): 245–257.

Moret P (2005) Los coléopteros Carabidae del páramo en los Andes del Ecuador: Sistemática, ecología y biogeografía. Monografía 2: 306 pp. [Museo de Zoología, Pontifica Universidad Católica del Ecuador, Quito, Ecuador]

Nascimento FF, Reis MD, Yang Z (2017) A biologist's guide to Bayesian phylogenetic analysis. Nature Ecology & Evolution 1: 1446–1454. https://doi.org/10.1038/s41559-017-0280-x

Nixon KC (2002) WinClada (a computer program for manipulating cladistic data and examining trees). Ithaca, NY. http://www.cladistics.com

Rambaut A, Drummond AJ, Xie D, Baele, Suchard MA (2018) Posterior summarisation in Bayesian phylogenetics using Tracer 1.7. Systematic Biology 67: 901–904. https://doi.org/10.1093/sysbio/syy032

Roig-Juñent S (2000) The subtribes and genera of the tribe Broscini (Coleoptera: Carabidae): cladistic analysis, taxonomic treatment, and biogeographical implications. Bulletin of the American Museum of Natural History 255: 1–90. https://doi.org/10.1206/0003-0090(2000)255<0001:TSAGOT>2.0.CO;2

Roig-Juñent S (2004) Los Migadopini (Coleoptera: Carabidae) de América del Sur: descripcíon de las estructuras genitales masculinas y femininas y consideraciones filogenéticas biogeográficas. Acta Entomologia Chilena 28: 7–29.

Ronquist F, Van Der Mark P, Huelsenbeck JP (2009) Bayesian phylogenetic analysis using MRBAYES. In: The Phylogenetic Handbook: A Practical Approach to Phylogenetic Analysis and Hypothesis Testing (eds P Lemey, M Salemi & A-M Vandamme). Cambridge University Press, Cambridge, 210–266. https://doi.org/10.1017/CBO9780511819049.009

Ronquist F, Teslenko M, van der Mark P, Ayres DL, Darling A, Höhna S, Larget B, Liu L, Suchard MA, Huelsenbeck JP (2012) MrBayes 3.2: efficient Bayesian phylogenetic inference and model choice across a large model space. Systematic Biology 61: 539–542. https://doi.org/10.1093/sysbio/sys029

Sanmartín I, Ronquist F (2004) Southern hemisphere biogeography inferred by event-based models: plant versus animal patterns. Systematic Biology 53: 206–243. https://doi.org/10.1080/10635150490423430

Scott JM, Turnbull IM, Auer A, Palin JM (2013) The sub-Antarctic Antipodes Volcano: a <0.5 Ma HIMU-like Surtseyan volcanic outpost on the edge of the Campbell Plateau, New Zealand. New Zealand Journal of Geology and Geophysics 56: 134–153 https://doi.org/10.1080/00288306.2013.802246

Sweney WJ (1980) Insects of Mount Cook National Park. M.S. thesis, University of Canterbury, Lincoln College, 328 pp. https://hdl.handle.net/10182/4038

Thompson RG (1979) Larvae of North American Carabidae with a key to the tribes. In: Erwin TL, Ball GE, Whitehead DR, Halpern AL (Eds) Carabid Beetles: Their Evolution, Natural History, and Classification, Dr W Junk Publishers, The Hague, The Netherlands, 209–291. https://doi.org/10.1007/978-94-009-9628-1_11

Trueman JWH, Pfeil BF, Kelchner SA, Yeates DK (2004) Did stick insects really regain their wings? Systematic Entomology 20: 138–139. https://doi.org/10.1111/j.0307-6970.2004.00251.x

Wegener A (1924) The Origins of Continents and Oceans (translated from the third German edition by Skerl JGA). EP Dutton and Company Publishers, New York, xx + 212 pp.

Whiting MF, Bradler S, Maxwell T (2003) Loss and recovery of wings in stick insects. Nature 421 (16 January 2003): 264–267. https://doi.org/10.1038/nature01313

Will KW (2020) Phylogeny and classification of the genus-group taxa of Loxandrina (Coleoptera, Carabidae, Abacetini). Deutsche Entomologische Zeitschrift 67(2): 151–182. https://doi.org/10.3897/dez.67.55985

Yu Y, Harris AJ, Blair C, He X (2015) RASP (Reconstruct Ancestral State in Phylogenies): a tool for historical biogeography. Molecular Phylogenetics and Evolution 87: 46–49. https://doi.org/10.1016/j.ympev.2015.03.008

Yu Y, Blair C, He X (2019) RASP 4: Ancestral State Reconstruction too for multiples genes and characters. Molecular Biology and Evolution 37(2): 604–606. https://doi.org/10.1093/molbev/msz257

Supplementary material 1

Data matrix exported as an SS file from Winclada (Nixon 2002) data file used for cladistic analysis

Authors: James K. Liebherr, Sergio Roig-Juñent, Kipling W. Will

Data type: pdf

Link: https://doi.org/10.3897/dez.71.134268.suppl1

Supplementary material 2

Majority-rule consensus of post-burn-in trees showing Bayesian posterior probabilities (PP) of all clades

Authors: James K. Liebherr, Sergio Roig-Juñent, Kipling W. Will

Data type: pdf

Explanation note: Resolution of this tree should be compared to Fig. 5 (see text).

Link: https://doi.org/10.3897/dez.71.134268.suppl2